Kindly please note this paper is published on:
Applied Mathematics and Computation, vol.399, article number: 126016, 15 June 2021

A comparative study of the dynamics of a three-disk dynamo system with and without time delay

Shuning Deng[1], Jinchen Ji[2], Guilin Wen[1,3,*], Huidong Xu[4]

[1]State Key Laboratory of Advanced Design and Manufacture for Vehicle Body, Hunan University, Changsha, Hunan 410082, China
[2]School of Mechanical and Mechatronic Engineering, University of Technology Sydney, Ultimo, NSW 2007, Australia
[3]School of Mechanical and Electric Engineering, Guangzhou University, Guangzhou, Guangdong 510006, China
[4]College of Mechanical and Vehicle Engineering, Taiyuan University of Technology, Taiyuan, Shanxi 030024, China

Abstract: The disk dynamo plays an important role in studying the geodynamo and much research works have been devoted to the understanding of dynamo dynamics. This paper further investigates an extended disk dynamo system having three coupled conducting disks and incorporates the interaction-induced time delay in the dynamic governing equations. By carrying out a comparative analysis, the dynamic behaviors of the coupled three-disk dynamo system with and without time delay are studied to explore novel and complex nonlinear dynamic phenomena in the coupled delayed dynamo system. It is found that the double Hopf bifurcations can be induced in the time-delayed dynamo system. Three different topological structures of the unfolding are obtained under different time delays. Accordingly, it is shown that the novel dynamic behaviors, including quasi-periodic torus, three-dimensional torus and the coexistence of multiple attractors, can appear in the time-delayed dynamo system. Furthermore, by performing the continuation analysis on the periodic orbit generated from the Hopf bifurcation of equilibrium, some new coexistence patterns, e.g., the

*Corresponding author.

E-mail address: glwen@hnu.edu.cn; glwen@gzhu.edu.cn (Guilin Wen)

coexistence of periodic orbits and chaos, the coexistence of quasi-periodic orbits and chaos, are observed in the dynamo system with time delay. Based on the obtained results, it is believed that the inclusion of time delay in the modelling of the three-disk dynamo system is necessary and meaningful for developing an in-depth understanding of dynamo dynamics. Finally, the results of theoretical analyses are verified by the numerical simulations.

Key Words: Three-disk dynamo; Time delay; co-dimension two bifurcations; Coexistence of multiple attractors; Chaos.

*Corresponding author.

E-mail address: glwen@hnu.edu.cn; glwen@gzhu.edu.cn (Guilin Wen)

1 Introduction

The disk dynamo is a simple yet effective mechanical model for explaining the geographical phenomenon of the irregular reversal of Earth's magnetic pole. Thus, it has attracted much attention in the fields of geophysics and mathematics. In 1955, Bullard [1] firstly considered a homopolar dynamo as a possible analogy to the homogenous fluid dynamo of the earth, and studied the stability of a single disk system. In 1958, Rikitake [2] analyzed a coupled two-disk dynamo model and observed the reversal phenomenon of electric current and magnetic field in the system. In 1972, Cook [3] modified the governing equations of a two-disk dynamo model by considering the two major factors in the geodynamo, i.e., viscous friction and time delay. Later, extensive research works on modeling, dynamics analysis, motion control and circuit experiment were conducted for a further understanding of such systems. For example, a single-disc dynamo model with extra coil current considered in the modeling was studied in Ref. [4], showing that the non-periodic reversal behavior could occur in the simple dynamo model. A dynamo model with the azimuthal current of disc considered was proposed in Ref. [5]. The arrangement hierarchy of a series of self-exciting Faraday-disk homopolar dynamos was discussed in Ref. [6]. The bifurcations of equilibrium points in a self-exciting Faraday disk homopolar dynamo model with quadratic motor were studied in Ref. [7], where the Hopf bifurcation and double-zero bifurcations were observed in the system. The Hopf bifurcation of a two-disc dynamo model with viscous friction and time delays was studied in Ref. [8]. The global dynamics of a Rikitake system were investigated in Ref. [9], in which the similarity between the Lorenz-like attractor and the Rikitake attractor was discussed. Moreover, the chaotic attractors [10-12] and circuit simulations [13-14] of various disk dynamo systems were also considered.

Time delay as an inherent and non-ignorable factor can have significant effects on the linear stabilities and nonlinear responses of various dynamic systems. For example, time delay can change the stability of the trivial equilibrium of a dynamic system even when the value of time delay is small [15], and induce novel co-dimensional bifurcations of equilibrium [16]. Moreover, the chaotic behavior can occur even in the first-order dynamic systems [17], while such phenomenon cannot be observed in the corresponding systems without time delay. Although the time delay can deteriorate the performances of dynamic systems in most cases, the intentionally introduced time delay could be beneficial to the design of absorbers and isolators [18-20], as well as the stabilization and control of the undesired motions [21-23]. Generally, the dynamic responses of the dynamic systems without time delay (described by ordinary differential equations) are different from the behaviors appearing in the delayed systems governed by the functional differential equations [24-25].

Recently, many studies are focused on the dynamics analysis of various delayed systems. For example, a single degree-of-freedom swing equation with a delayed damping term only was studied in Ref. [26] and a variety of bifurcation behaviors were observed in the delayed equation. The classical Duffing oscillator with the delayed damping term was investigated in Ref. [27] and the delay-induced resonance was addressed. In addition, a two-dimensional gut microbiota model with measurement delays was studied in Ref. [28], where a specific type of co-dimension two bifurcation (non-resonant double Hopf bifurcation) was noted. A two-dimensional Lengyel-Epstein chemical reaction model with the time delay in the self-decomposition of the activator was investigated in Ref. [29], where the stability switches of equilibrium were observed. A three-dimensional tumor-immune

competitive model with single interaction delay was proposed in Ref. [30] and the linear stability and the co-dimension one Hopf bifurcation of the equilibria were examined.

Although extensive researches have been carried out on the dynamics analysis of delayed dynamic systems, little attentions have been paid on studying the influence of time delay on the dynamic behaviors of these systems. To bridge this gap, this paper aims to investigate the effect of time delay on the dynamics of a three-disk dynamo system. The contributions of this work are in the following aspects. First, a three-disk dynamo system with viscous friction and time delay is proposed and studied in this paper. Such a three-disk dynamo system with viscous friction and time delay has not been studied yet in the literature, due to the complexity on the theoretical analysis and numerical simulation of high-dimensional functional differential equations describing the delayed dynamo system. Second, novel delay-induced double Hopf bifurcations are observed in the disk dynamo system and different unfolding structures are obtained to show the rich dynamic behaviors of the system. Third, the secondary bifurcations and transitions between complex responses resulting from the Hopf bifurcation of equilibrium are illustrated in the delayed three-disk dynamo system. This work can be considered as a valuable contribution to the understanding of the mechanism of the multiple coupled disks dynamo system.

The remainder of this paper is divided into six sections. The governing equations of the three-disk dynamo model with viscous friction and time delay are briefly introduced in Section 2. In Section 3, the dynamics of the three-disk dynamo system in the absence of time delay is studied to examine the stability and possible bifurcations of equilibria. It is found that only two types of co-dimension one bifurcations, i.e., the pitchfork and Hopf bifurcations, can occur on the stability

boundaries of equilibria for the non-delay case. The stability and co-dimension one bifurcations of equilibria for the delayed three-disk dynamo system are studied in Section 4. Some specific intersection points are observed on the stability boundaries of equilibriums, indicating the occurrence of co-dimension two bifurcations in the delayed system. The detailed analysis of the possible co-dimension two bifurcations of equilibrium is presented in Section 5. Furthermore, Section 6 illustrates the chaotic motions and some new nonlinear phenomena in the delayed dynamo system. Finally, conclusions are given in Section 7.

2 The mechanical model and the governing equations

The disk dynamo model studied in this paper is shown in Fig. 1, where three disk dynamos are coupled to each other. The magnetic field of the conducting disk (the second and third disks) is induced by the current of its left disk and the magnetic field of the first disk is induced by the current of the third. As described in Ref. [10], the governing equations of the three-disk dynamo system can be written as:

$$\begin{cases} \dot{x}_1 = -kx_1 + y_1 x_3 \\ \dot{x}_2 = -kx_2 + y_2 x_1 \\ \dot{x}_3 = -kx_3 + y_3 x_2 \\ \dot{y}_1 = 1 - x_1 x_3 \\ \dot{y}_2 = 1 - x_2 x_1 \\ \dot{y}_3 = 1 - x_3 x_2 \end{cases} \tag{1}$$

where x_1, x_2 and x_3 are the electric currents in the disks, y_1, y_2 and y_3 are the angular velocities and k represents the Ohmic dissipation coefficient. Cook [3] introduced the viscous friction and the time delay in a classical two-disk Rikitake model to better describe the geodynamo. For the same reason, the two factors are also considered in the three-disk dynamo model governed by Eq. (1). Accordingly, the dynamic equations of the three-disk dynamo system can be extended to:

$$\begin{cases} \dot{x}_1 = -kx_1 + y_1 x_3(t-\tau) \\ \dot{x}_2 = -kx_2 + y_2 x_1(t-\tau) \\ \dot{x}_3 = -kx_3 + y_3 x_2(t-\tau) \\ \dot{y}_1 = 1 - x_1 x_3(t-\tau) - cy_1 \\ \dot{y}_2 = 1 - x_2 x_1(t-\tau) - cy_2 \\ \dot{y}_3 = 1 - x_3 x_2(t-\tau) - cy_3 \end{cases} \tag{2}$$

where, in comparison with Eq. (1), the newly introduced terms $-cy_i$, $i = 1,2,3$ represent the viscous frictions in the disks and c denotes the coefficient of friction. τ designates the interaction delay caused by the electromagnetic diffusion [3]. For the sake of convenience, $\mu = \mu(c,k)$ is chosen as the main bifurcation parameter and τ is set as the auxiliary parameter, with their ranges of $c \in (0,2]$, $k \in [0,2]$ and $\tau \in [0,2]$.

By letting the left hand sides of Eq. (2) be zero and solving the resultant algebraic equations, three possible equilibrium points are obtained for the three-disk dynamo system. The distribution of these equilibria in the (c,k) plane is shown in Fig. 2, where the three equilibria are given by

$$\begin{aligned} E_0 &= (0,0,0,\frac{1}{c},\frac{1}{c},\frac{1}{c}), \\ E_{1,2} &= (\pm\sqrt{-ck+1},\pm\sqrt{-ck+1},\pm\sqrt{-ck+1},k,k,k) \end{aligned} \tag{3}$$

Here $E_{1,2}$ can be considered as symmetric equilibrium points. It is noted that the curve P in Fig. 2 satisfies

$$P: \quad ck = 1 \tag{4}$$

Due to the symmetry $(x_1,x_2,x_3,y_1,y_2,y_3) \to (-x_1,-x_2,-x_3,y_1,y_2,y_3)$, the dynamic responses near the pair of symmetric equilibrium points $E_{1,2}$ are similar. For the sake of simplicity, E_1 is chosen as the equilibrium in the following analysis and the system response near equilibrium E_2 can be easily investigated in a same way.

The above-mentioned equilibria can be transformed into the origin by setting $u_1 = x_1 - x_{10},\ u_2 = x_2 - x_{20},\ u_3 = x_3 - x_{30},\ u_4 = y_1 - y_{10},\ u_5 = y_2 - y_{20},\ u_6 = y_3 - y_{30}$, where $(x_{10}, x_{20}, x_{30}, y_{10}, y_{20}, y_{30})$ are determined by the equilibria given in Eq. (3). Thus, Eq. (2) can be rewritten as

$$\begin{cases} \dot{u}_1 = -ku_1 + x_{30}u_4 + y_{10}u_{3\tau} + u_4u_{3\tau} + (x_{30}y_{10} - kx_{10}) \\ \dot{u}_2 = -ku_2 + x_{10}u_5 + y_{20}u_{1\tau} + u_5u_{1\tau} + (x_{10}y_{20} - kx_{20}) \\ \dot{u}_3 = -ku_3 + x_{20}u_6 + y_{30}u_{2\tau} + u_6u_{2\tau} + (x_{20}y_{30} - kx_{30}) \\ \dot{u}_4 = 1 - x_{30}u_1 - cu_4 - x_{10}u_{3\tau} - u_1u_{3\tau} - (x_{10}x_{30} + cy_{10}) \\ \dot{u}_5 = 1 - x_{10}u_2 - cu_5 - x_{20}u_{1\tau} - u_2u_{1\tau} - (x_{20}x_{10} + cy_{20}) \\ \dot{u}_6 = 1 - x_{20}u_3 - cu_6 - x_{30}u_{2\tau} - u_3u_{2\tau} - (x_{30}x_{20} + cy_{30}) \end{cases} \tag{5}$$

Furthermore, Eq. (5) can be expressed in a compact form as:

$$\dot{X} = F(\mu, X, X(t-\tau)) \tag{6}$$

where $X = (u_1\ u_2\ u_3\ u_4\ u_5\ u_6)^T$, $F(\mu, X, X(t-\tau))$ represents the right-hand side terms of Eq. (5), and $\mu = \mu(c,k)$ is the bifurcation parameter. In the subsequent sections, the linear stability and nonlinear dynamic behaviors of the delayed three-disk dynamo system (6) will be studied. Two cases, i.e., $\tau = 0$ and $\tau > 0$, will be addressed.

3 Stabilities and co-dimension one bifurcations of equilibria with $\tau = 0$

When the time delay is neglected in the three-disk dynamo system (6), the governing equations can be simplified to a set of ordinary differential equations:

$$\dot{X} = F(\mu, X) \tag{7}$$

Based on the governing equation (7), the stabilities and possible bifurcations of equilibria E_0 and E_1 will be analyzed in the following subsections.

3.1 Stability and pitchfork bifurcation of equilibrium E_0

Linearizing Eq. (7) and substituting the variables $(x_{10}, x_{20}, x_{30}, y_{10}, y_{20}, y_{30})$ by equilibrium E_0, results in a polynomial characteristic equation:

$$g_0\lambda^6 + g_1\lambda^5 + g_2\lambda^4 + g_3\lambda^3 + g_4\lambda^2 + g_5\lambda + g_6 = 0 \tag{8}$$

where

$$g_0 = 1,\ g_1 = 3c + 3k,\ g_2 = 3c^2 + 9ck + 3k^2,\ g_3 = c^3 + 9c^2k + 9ck^2 + k^3 - \frac{1}{c^3},$$
$$g_4 = 3c^3k + 9c^2k^2 + 3ck^3 - \frac{3}{c^2},\ g_5 = 3c^3k^2 + 3c^2k^3 - \frac{3}{c},\ g_6 = c^3k^3 - 1.$$

By applying the Routh-Hurwitz criterion, the stability region of equilibrium E_0 can be determined, as the gray area shown in Fig. 3(a). On the boundary P determined by Eq. (4), a zero eigenvalue of Eq. (8) appears and this indicates the occurrence of the pitchfork bifurcation. To briefly verify the static bifurcation, the bifurcation diagram is drawn near the bifurcation point PB in Fig. 3(a) and shown in Fig. 3(b). The theoretical predictions obtained from Eq. (3) are also presented in Fig. 3(b). It is easy to notice that the theoretical predictions agree well with the numerical simulations.

3.2 Stability and pitchfork bifurcation of equilibrium E_1

Similarly, the linear stability of Eq. (7) at equilibrium E_1 can be determined by studying the following polynomial characteristic equation:

$$g_0'\lambda^6 + g_1'\lambda^5 + g_2'\lambda^4 + g_3'\lambda^3 + g_4'\lambda^2 + g_5'\lambda + g_6' = 0 \tag{9}$$

where

$$g_0' = 1,\ g_1' = 3c + 3k,\ g_2' = 3c^2 + 6ck + 3k^2 + 3,\ g_3' = c^3 + 3c^2k + 3ck^2 + 6c + 6k,$$
$$g_4' = -6ck^3 + 3c^2 + 6ck + 6k^2 + 3,\ g_5' = -12c^2k^3 + 12ck^2 + 3c,$$
$$g_6' = -8c^3k^3 + 12c^2k^2 - 6ck + 2.$$

According to the Routh-Hurwitz criterion, the stability region of equilibrium E_1 is obtained as the gray area shown in Fig. 3(c). Pitchfork bifurcation occurs on the

stability boundary P determined by Eq. (4) and the discussion on the pitchfork bifurcation is omitted here for brevity. Notably, there is only the curve P with zero eigenvalue satisfied in the case. In addition to the boundary of zero eigenvalue, the boundary with a pair of purely imaginary eigenvalues $\pm i\omega_0, \omega_0 \neq 0$ is found and marked by the blue solid line in Fig. 3(c), which indicates the occurrence of Hopf bifurcations if the eigenvalues satisfy the transversality condition.

3.3 Hopf bifurcation analysis of equilibrium E_1

To identify the generic Hopf bifurcation occurring on the stability boundary of equilibrium E_1 in Fig. 3(c), the method of multiple scales (MMS) [31-32] is applied to obtain the approximate solutions and the corresponding standard normal form.

According to the MMS, the solution of Eq. (7) can be assumed as

$$X(t;\varepsilon) = \sum_{m=1}^{3} \varepsilon^m X_m(T_0, T_2) \tag{10}$$

where $\varepsilon << 1$ is a small parameter and $T_i = \varepsilon^i t,\ i = 0, 2$ are the independent time scales. In the small neighborhood of bifurcation point k_0, the bifurcation parameter k can be expressed as:

$$k = k_0 + k_\varepsilon, \quad k_\varepsilon = \varepsilon^2 \hat{k}_\varepsilon \tag{11}$$

Substituting Eq. (10) and Eq. (11) into Eq. (7) and equating the coefficients of like powers of ε, yields

$$\begin{aligned} O(\varepsilon):&\quad D_0 X_1 - F_X^0 X_1 = 0 \\ O(\varepsilon^2):&\quad D_0 X_2 - F_X^0 X_2 = \frac{1}{2} F_{XX}^0 X_1^2 \\ O(\varepsilon^3):&\quad D_0 X_3 - F_X^0 X_3 = F_{Xk_\varepsilon}^0 X_1 \hat{k}_\varepsilon - D_2 X_1 + F_{XX}^0 X_1 X_2 \end{aligned} \tag{12}$$

Here, $D_i = \partial / \partial T_i$ is the differential operator, and $F_{XX}^0 = \dfrac{\partial^2 F(0,0)}{\partial X^2}$, $F_{Xk_\varepsilon}^0 = \dfrac{\partial^2 F(0,0)}{\partial X \partial k_\varepsilon}$ represent the derivatives of the right-hand side term of Eq. (7) with respect to the state

variables and the bifurcation parameter.

For the first equation of Eq. (12), the general solution can be expressed as

$$X_1 = M p_1 e^{i\omega_0 T_0} + cc \tag{13}$$

where cc is the complex conjugate of the preceding term, M denotes the amplitude function, and p_1 stands for the right eigenvector of F_X^0 corresponding to the eigenvalue $i\omega_0$. The vector p_1 is given by

$$p_1 = (p_{11} \quad p_{12} \quad p_{13} \quad p_{14} \quad p_{15} \quad p_{16})^T$$

$$\begin{aligned}
&p_{11} = \frac{\alpha_2\alpha_3 - \alpha_4^2}{\alpha_1\alpha_2 + \alpha_4^2}, \quad p_{12} = \frac{\alpha_2^2\alpha_3^2 - 2\alpha_2\alpha_3\alpha_4^2 + \alpha_4^4}{\alpha_1^2\alpha_2^2 + 2\alpha_1\alpha_2\alpha_4^2 + \alpha_4^4}, \quad p_{13} = 1, \\
&p_{14} = -\frac{\alpha_1\alpha_4 + \alpha_3\alpha_4}{\alpha_1\alpha_2 + \alpha_4^2}, \quad p_{15} = \frac{-\alpha_1\alpha_2\alpha_3\alpha_4 + \alpha_1\alpha_4^3 - \alpha_2\alpha_4\alpha_3^2 + \alpha_3\alpha_4^3}{\alpha_1^2\alpha_2^2 + 2\alpha_1\alpha_2\alpha_4^2 + \alpha_4^4}, \\
&p_{16} = \frac{\alpha_1^3\alpha_2^2 + 2\alpha_2\alpha_1^2\alpha_4^2 + \alpha_1\alpha_4^2 - \alpha_2^2\alpha_3^3 + 2\alpha_2\alpha_3^2\alpha_4^2 - \alpha_3\alpha_4^4}{\alpha_4\alpha_1^2\alpha_2^2 + 2\alpha_1\alpha_2\alpha_4^3 + \alpha_4^5}
\end{aligned} \tag{14}$$

where $\alpha_1 = i\omega_0 + k_0$, $\alpha_2 = i\omega_0 + c$, $\alpha_3 = k_0$, $\alpha_4 = \sqrt{-ck_0 + 1}$. Additionally, the left eigenvector q_1 of F_X^0, which will be used for the elimination of the secular terms, is calculated as

$$q_1 = G \cdot (q_{11} \quad q_{12} \quad q_{13} \quad q_{14} \quad q_{15} \quad q_{16})^T$$

$$\begin{aligned}
&q_{11} = \frac{(\alpha_4\overline{\alpha}_4 - \overline{\alpha}_2\overline{\alpha}_3)^2}{(\alpha_4^2 + \overline{\alpha}_1\overline{\alpha}_2)^2}, \quad q_{12} = \frac{-\alpha_4\overline{\alpha}_4 + \overline{\alpha}_2\overline{\alpha}_3}{\alpha_4^2 + \overline{\alpha}_1\overline{\alpha}_2}, \quad q_{13} = 1, \\
&q_{14} = \frac{\alpha_4(\alpha_4\overline{\alpha}_4 - \overline{\alpha}_2\overline{\alpha}_3)^2}{\overline{\alpha}_2(\alpha_4^2 + \overline{\alpha}_1\overline{\alpha}_2)^2}, \quad q_{15} = \frac{-\alpha_4^2\overline{\alpha}_4 + \overline{\alpha}_2\overline{\alpha}_3\alpha_4}{\overline{\alpha}_2\alpha_4^2 + \overline{\alpha}_1\overline{\alpha}_2^2}, \quad q_{16} = \frac{\alpha_4}{\overline{\alpha}_2}
\end{aligned} \tag{15}$$

Under the orthogonality condition of $q_1^H p_1 = 1$, the coefficient G is computed as:

$$\overline{G} = (\frac{(-\alpha_2\alpha_3 + |\alpha_4|^2)^2(\alpha_2\alpha_3 - \alpha_4^2)}{(\alpha_1\alpha_2 + \overline{\alpha}_4^2)^2(\alpha_1\alpha_2 + \alpha_4^2)} - \frac{(-\alpha_2\alpha_3 + |\alpha_4|^2)(\alpha_2\alpha_3 - \alpha_4^2)^2}{(\alpha_1\alpha_2 + \alpha_4^2)^2(\alpha_1\alpha_2 + \overline{\alpha}_4^2)}$$
$$+ \frac{\overline{\alpha}_4(\alpha_1^3\alpha_2^2 + 2\alpha_2\alpha_1^2\alpha_4^2 + \alpha_1\alpha_4^4 - \alpha_3^3\alpha_2^2 + 2\alpha_2\alpha_3^2\alpha_4^2 - \alpha_3\alpha_4^4)}{\alpha_2\alpha_4(\alpha_1\alpha_2 + \alpha_4^2)^2}$$
$$+ \frac{\overline{\alpha}_4(-\alpha_2\alpha_3 + |\alpha_4|^2)(\alpha_1\alpha_2\alpha_3\alpha_4 - \alpha_1\alpha_4^3 + \alpha_2\alpha_4\alpha_3^2 - \alpha_3\alpha_4^3)}{\alpha_2(\alpha_1\alpha_2 + \overline{\alpha}_4^2)(\alpha_1\alpha_2 + \alpha_4^2)^2}$$
$$- \frac{\overline{\alpha}_4(-\alpha_2\alpha_3 + |\alpha_4|^2)^2(\alpha_1\alpha_4 + \alpha_3\alpha_4)}{\alpha_2(\alpha_1\alpha_2 + \alpha_4^2)(\alpha_1\alpha_2 + \overline{\alpha}_4^2)^2} + 1)^{-1}$$

Substituting Eq. (13) into the second equation of Eq. (12) leads to

$$D_0X_2 - F_X^0X_2 = \frac{1}{2}F_{XX}^0p_1^2M^2e^{2i\omega_0T_0} + \frac{1}{2}F_{XX}^0p_1\overline{p}_1M\overline{M} + cc \tag{16}$$

The particular solution of Eq. (16) is given by

$$X_2 = z_1M^2e^{2i\omega_0T_0} + z_2M\overline{M} + cc \tag{17}$$

where z_1 and z_2 can be determined from $(2i\omega_0E - F_X^0)z_1 = \frac{1}{2}F_{XX}^0p_1^2$, $(-F_X^0)z_2 = \frac{1}{2}F_{XX}^0p_1\overline{p}_1$, respectively. Here, E represents the identity matrix.

Substituting Eq. (13) and Eq. (17) into the third equation of Eq. (12) and then eliminating the secular terms in the resultant equation leads to the equation involved with the derivative D_2M . The standard normal form of the generic Hopf bifurcation can then be obtained by using the derived expression from D_2M and absorbing the perturbation parameter ε [32], which is given by

$$\dot{M} = C_{1\mu}(k_\varepsilon)M + C_{11\bar{1}}M^2\overline{M} \tag{18}$$

Here, $C_{1\mu}(k_\varepsilon) = q_1^HF_{Xk_\varepsilon}^0k_\varepsilon p_1$ is a function of the perturbation parameter k_ε, and $C_{11\bar{1}} = q_1^H(F_{XX}^0(p_1\bar{z}_2 + z_1\overline{p}_1 + z_2p_1))$ is a constant determined by the Hopf bifurcation point. By setting $M = \rho e^{i\theta}$, Eq. (18) can be rewritten in polar form as:

$$\dot{\rho} = R_1(k_\varepsilon)\rho + R_{11\bar{1}}\rho^3 \tag{19}$$

where $R_1(k_\varepsilon)=\mathrm{Re}(C_{1\mu}(k_\varepsilon))$ and $R_{11\bar{1}}=\mathrm{Re}(C_{11\bar{1}})$. The phase equation is not presented here for brevity. The characteristics of the bifurcated periodic orbits, i.e., direction and stability, can be theoretically determined from Eq. (19). To verify the theoretical analysis, a bifurcation diagram near the point CH in Fig. 3(c) is drawn in Fig. 3(d). At the bifurcation point CH, the coefficients of Eq. (19) are calculated as $R_1(k_\varepsilon)\approx -0.865703\,k_\varepsilon$ and $R_{11\bar{1}}\approx -1.636170$. Therefore, the bifurcated periodic orbits which exist for $k_\varepsilon<0$ are stable. The theoretically predicted radius of the stable periodic orbit in terms of the bifurcation parameter k can be obtained as

$$r\approx\delta\sqrt{-0.529103\,k+0.145474} \tag{20}$$

where δ is a scalar coefficient and is given by

$$\delta=\frac{1}{2\pi}\int_0^{2\pi}\sqrt{\sum_{j=1}^{6}(p_{1j}\,e^{i\theta}+\bar{p}_{1j}\,e^{-i\theta})^2}\,d\theta$$

The corresponding δ for the bifurcation point CH is obtained as 3.626554. From Fig. 3(d), it can be seen that the theoretical predictions are in good agreement with the numerical simulations.

4 Stabilities and co-dimension one bifurcations of equilibria with $\tau>0$

In this section, the stabilities and bifurcations of equilibria E_0 and E_1 are investigated in the three-disk dynamo system (6) with $\tau>0$. In order to explore the transition of stability boundaries of the equilibria with respect to the time delay, a series of discrete time delays, i.e., $\tau=0.5,\ 1,\ 1.5,\ 2$, are chosen for the subsequent analysis. The realization of the numerical calculation of the delayed dynamo system (6) is based on the fourth-order Runge-Kutta method with fixed integration step [23].

4.1 Stability and pitchfork bifurcation of equilibrium E_0

The transcendental characteristic equation for the case of $\tau > 0$ can be obtained by linearizing Eq. (6) and substituting the trial solution $X = \overline{X}e^{\lambda t}$ into the resultant equation. For equilibrium E_0, the characteristic equation is given by:

$$D(\lambda,\tau) = P(\lambda) + Q(\lambda)e^{-3\lambda\tau} = 0 \tag{21}$$

where

$$\begin{aligned} P(\lambda) &= \lambda^6 + (3c+3k)\lambda^5 + (3c^2+9ck+3k^2)\lambda^4 + (c^3+9c^2k+9ck^2 \\ &\quad + k^3)\lambda^3 + (3c^3k+9c^2k^2+3ck^3)\lambda^2 + (3c^3k^2+3c^2k^3)\lambda + c^3k^3, \\ Q(\lambda) &= -\frac{\lambda^3}{c^3} - \frac{3\lambda^2}{c^2} - \frac{3\lambda}{c} - 1. \end{aligned}$$

The equilibrium E_0 is asymptotically stable when all the eigenvalues of Eq. (21) have negative real parts. By assuming purely imaginary eigenvalue $\lambda = i\omega,\ \omega \geq 0$ and substituting it into Eq. (21), the corresponding frequency equations can be derived by separating the real and imaginary parts as:

$$\begin{cases} f_1(c,k,\omega) = -\omega^6 + (3c^2+9ck+3k^2)\omega^4 + \dfrac{\sin(3\omega\tau)}{c^3}\omega^3 + (\dfrac{3\cos(3\omega\tau)}{c^2} - 3c^3k \\ \qquad\qquad - 9c^2k^2 - 3ck^3)\omega^2 - \dfrac{3\sin(3\omega\tau)}{c}\omega + c^3k^3 - \cos(3\omega\tau) = 0, \\ f_2(c,k,\omega) = (3c+3k)\omega^5 + (\dfrac{\cos(3\omega\tau)}{c^3} - c^3 - 9c^2k - 9ck^2 - k^3)\omega^3 \\ \qquad\qquad - \dfrac{3\sin(3\omega\tau)}{c^2}\omega^2 + (3c^3k^2 + 3c^2k^3 - \dfrac{3\cos(3\omega\tau)}{c})\omega + \sin(3\omega\tau) = 0. \end{cases} \tag{22}$$

From Eq. (22), it is easy to notice that the equality $ck = 1$ holds when $\omega = 0$, indicating the curve P with $ck = 1$ remains as the pitchfork bifurcation curve and the time delay does not have any effect on such bifurcation. The detailed analysis of the pitchfork bifurcation is given in the previous section. For other possible delay-induced stability boundaries in the two-parameter (c,k) plane, the D-subdivision method [33] is adopted here. The stability region of equilibrium E_0 with different delays are shown in Fig. 4(a), where the gray shadow region represents

the stable equilibrium E_0. It is seen that the stability region of equilibrium E_0 remains unchanged as the delay varies from the value of 0.5 to the value of 2.

4.2 Stability and co-dimension one bifurcations of equilibrium E_1

The stability of equilibrium E_1 is determined by the following transcendental characteristic equation:

$$D(\lambda,\tau)=P(\lambda)+Q(\lambda)e^{-3\lambda\tau}=0$$

where

$$\begin{aligned}P(\lambda)&=\lambda^6+(3c+3k)\lambda^5+(3c^2+6ck+3k^2+3)\lambda^4+(c^3+3c^2k+3ck^2+k^3+6c\\&\quad+6k)\lambda^3+(3c^2+6ck+3k^2+3)\lambda^2+(3c+3k)\lambda+1,\\Q(\lambda)&=-k^3\lambda^3+(3k^2-6ck^3)\lambda^2+(12ck^2-12c^2k^3-3k)\lambda+(12c^2k^2-8c^3k^3-6ck+1).\end{aligned}\tag{23}$$

Similarly, substituting $\lambda=i\omega,\ \omega\geq 0$ into Eq. (23) yields the following frequency equations:

$$\begin{cases}f_1(c,k,\omega)=-\omega^6+(3c^2+6ck+3k^2+3)\omega^4+k^3\sin(3\omega\tau)\omega^3+(6ck^3\cos(3\omega\tau)\\\qquad\qquad-3k^2\cos(3\omega\tau)-3c^2-6ck-3k^2-3)\omega^2+(12ck^2-12c^2k^3\\\qquad\qquad-3k)\sin(3\omega\tau)\omega+(12c^2k^2-8c^3k^3-6ck+1)\cos(3\omega\tau)+1=0,\\f_2(c,k,\omega)=(3c+3k)\omega^5+(k^3\cos(3\omega\tau)-c^3-3c^2k-3ck^2-k^3-6c-6k)\omega^3\\\qquad\qquad+(3k^2-6ck^3)\sin(3\omega\tau)\omega^2+((12ck^2-12c^2k^3-3k)\cos(3\omega\tau)+3c\\\qquad\qquad+3k)\omega+(8c^3k^3-12c^2k^2+6ck-1)\sin(3\omega\tau)=0.\end{cases}\tag{24}$$

Notably, $ck=1$ holds when $\omega=0$ in Eq. (24) and the curve P remains unchanged as the pitchfork bifurcation curve irrespective of the value of time delay. The D-subdivision method [33] is applied again to obtain the stability boundaries of equilibrium E_1 with different delays and the corresponding stable regions are shown in Figs. 4(b-e). Obviously, the time delay can lead to complicated stability boundaries of equilibrium E_1. Besides, the size and shape of the stability regions are changed as the time delay varies, indicating the phenomenon of stability switches of equilibrium

as shown in Fig. 5 where the stability of equilibrium switches twice.

Moreover, same as the co-dimension one bifurcations of equilibrium E_1 for the case of $\tau = 0$, the pitchfork and generic Hopf bifurcations can also occur in the delay case. The detailed analysis is omitted here to avoid the repetition of presentation. Differently, some specific intersection points are found on the stability boundaries of equilibrium E_1, which are indicated by the asterisks in Figs. 4(b-e). These points are the potential co-dimension two bifurcation points. The analysis of the system response near the newly appeared intersection points will be performed in the following section.

5 Delay-induced co-dimension two bifurcations of equilibrium E_1

As mentioned previously, the delay-induced intersection points are found on the stability boundaries of equilibrium E_1, where more bifurcation behaviors can be observed in the delayed dynamo system (6). The intersection points marked in Figs. 4(b-e) are associated with two pairs of purely imaginary eigenvalues and the corresponding bifurcations are termed as the double Hopf bifurcation [34]. It should be pointed out that the resonance condition is not satisfied at these double Hopf bifurcation points in Figs. 4(b-e). Next, the unfolding of all the double Hopf points in Figs. 4(b-e) will be studied by using MMS.

5.1 Unfolding of double Hopf bifurcations

In this study, the truncated third-order normal form is used to analyze the system response in the small neighborhood of the marked double Hopf bifurcation points in Figs. 4(b-e). By applying the MMS to the delayed system (6), the truncated third-order normal form of the double Hopf bifurcations can be expressed as [35]

$$\begin{aligned}\dot{M}_1 &= C_{1\mu}(\mu_\varepsilon)M_1 + C_{11\bar{1}}M_1^2\overline{M}_1 + C_{12\bar{2}}M_1M_2\overline{M}_2 \\ \dot{M}_2 &= C_{2\mu}(\mu_\varepsilon)M_2 + C_{1\bar{1}2}M_1\overline{M}_1M_2 + C_{22\bar{2}}M_2^2\overline{M}_2\end{aligned} \tag{25}$$

where $\mu_\varepsilon = \mu_\varepsilon(c_\varepsilon, k_\varepsilon)$ is the perturbation parameter and it is assumed as $\mu_\varepsilon = \varepsilon^2\hat{\mu}_\varepsilon$. By letting $M_i = \rho_i e^{i\theta_i}, i = 1, 2$, the corresponding amplitude equations can be obtained as:

$$\begin{aligned}\dot{\rho}_1 &= R_1\rho_1 + R_{11\bar{1}}\rho_1^3 + R_{12\bar{2}}\rho_1\rho_2^2 \\ \dot{\rho}_2 &= R_2\rho_2 + R_{1\bar{1}2}\rho_1^2\rho_2 + R_{22\bar{2}}\rho_2^3\end{aligned} \tag{26}$$

where $R_i = \mathrm{Re}(C_{i\mu}(\mu_\varepsilon)) = \alpha_{i1}c_\varepsilon + \alpha_{i2}k_\varepsilon$, $R_{ijk} = \mathrm{Re}(C_{ijk})$, and the coefficients α_{i1}, α_{i2} and R_{ijk} are the real numbers which are determined by the double Hopf bifurcation point. According to Eq. (26), the possible solutions and their corresponding existence conditions are

(C0) $N_0 : (\rho_1, \rho_2) = (0, 0)$ exists for all small perturbation parameters;

(C1) $N_1 : (\rho_1, \rho_2) = (\sqrt{-\frac{R_1}{R_{11\bar{1}}}}, 0)$ exists if $R_1R_{11\bar{1}} < 0$ holds and $L_1 : R_1R_{11\bar{1}} = 0$ represents the critical line;

(C2) $N_2 : (\rho_1, \rho_2) = (0, \sqrt{-\frac{R_2}{R_{22\bar{2}}}})$ exists if $R_2R_{22\bar{2}} < 0$ holds and $L_2 : R_2R_{22\bar{2}} = 0$ is the critical line;

(C3) $N_3 : (\rho_1, \rho_2) = (\sqrt{\frac{R_2R_{12\bar{2}} - R_1R_{22\bar{2}}}{R_{11\bar{1}}R_{22\bar{2}} - R_{1\bar{1}2}R_{12\bar{2}}}}, \sqrt{\frac{R_1R_{1\bar{1}2} - R_2R_{11\bar{1}}}{R_{11\bar{1}}R_{22\bar{2}} - R_{1\bar{1}2}R_{12\bar{2}}}})$ exists if and only if the following conditions hold:

$$\begin{cases}(R_2R_{12\bar{2}} - R_1R_{22\bar{2}})(R_{11\bar{1}}R_{22\bar{2}} - R_{1\bar{1}2}R_{12\bar{2}}) > 0 \\ (R_1R_{1\bar{1}2} - R_2R_{11\bar{1}})(R_{11\bar{1}}R_{22\bar{2}} - R_{1\bar{1}2}R_{12\bar{2}}) > 0\end{cases}$$

In this case, the corresponding critical lines are:

$$\begin{cases} L_3: (R_1 R_{1\bar{1}2} - R_2 R_{11\bar{1}})(R_{11\bar{1}} R_{22\bar{2}} - R_{1\bar{1}2} R_{12\bar{2}}) = 0 \\ L_4: (R_2 R_{12\bar{2}} - R_1 R_{22\bar{2}})(R_{11\bar{1}} R_{22\bar{2}} - R_{1\bar{1}2} R_{12\bar{2}}) = 0 \end{cases}$$

Here, solution N_0 corresponds to the equilibrium of the delayed system (6), N_1 and N_2 are associated with the periodic solutions with $\rho_2 = 0$ and $\rho_1 = 0$, respectively, while N_3 with $\rho_{1,2} > 0$ represents the quasi-periodic solution. The stability of N_i, $i = 0, 1, 2, 3$, can be studied based on the corresponding characteristic equation which is obtained by linearizing Eq. (26) at each solution

$$D(\lambda)\big|_{N_i} = (\lambda - (R_1 + 3R_{11\bar{1}}\rho_1^2 + R_{12\bar{2}}\rho_2^2))(\lambda - (R_2 + 3R_{22\bar{2}}\rho_2^2 + R_{1\bar{1}2}\rho_1^2)) - 4R_{1\bar{1}2}R_{12\bar{2}}\rho_1^2\rho_2^2 \tag{27}$$

The solution $N_i, i = 0, 1, 2, 3$ is stable if the real parts of all the eigenvalues of Eq. (27) are negative. Four cases (S0)-(S3) corresponding to the four solutions of Eq. (26) are discussed below as the stability conditions:

(S0) For solution N_0, the corresponding eigenvalues are

$$\lambda_1 = R_1, \quad \lambda_2 = R_2 \tag{28}$$

therefore, N_0 is stable if $R_1 < 0$ and $R_2 < 0$.

(S1) For the periodic solution N_1, the eigenvalues are

$$\lambda_1 = -2R_1, \quad \lambda_2 = R_2 - \frac{R_{1\bar{1}2}R_1}{R_{11\bar{1}}} \tag{29}$$

therefore, N_1 is stable if $R_1 > 0$ and $R_2 - \frac{R_{1\bar{1}2}R_1}{R_{11\bar{1}}} < 0$ are satisfied.

(S2) For the periodic solution N_2, the eigenvalues are

$$\lambda_1 = -2R_2, \quad \lambda_2 = R_1 - \frac{R_{12\bar{2}}R_2}{R_{22\bar{2}}} \tag{30}$$

therefore, N_2 is stable if $R_2 > 0$ and $R_1 - \frac{R_{12\bar{2}}R_2}{R_{22\bar{2}}} < 0$ are satisfied.

(S3) For the quasi-periodic solution N_3, the eigenvalues are

$$\lambda_{1,2} = \frac{(a'+b') \pm \sqrt{(a'+b')^2 - 4(a'b'-c'd')}}{2} \tag{31}$$

where

$$a' = \frac{2R_{11\bar{1}}(R_2R_{12\bar{2}} - R_1R_{22\bar{2}})}{R_{11\bar{1}}R_{22\bar{2}} - R_{1\bar{1}2}R_{12\bar{2}}}, \quad b' = \frac{2R_{22\bar{2}}(R_1R_{1\bar{1}2} - R_2R_{11\bar{1}})}{R_{11\bar{1}}R_{22\bar{2}} - R_{1\bar{1}2}R_{12\bar{2}}},$$

$$c' = 2R_{12\bar{2}}\sqrt{\frac{(R_2R_{12\bar{2}} - R_1R_{22\bar{2}})(R_1R_{1\bar{1}2} - R_2R_{11\bar{1}})}{(R_{11\bar{1}}R_{22\bar{2}} - R_{1\bar{1}2}R_{12\bar{2}})^2}},$$

$$d' = 2R_{1\bar{1}2}\sqrt{\frac{(R_2R_{12\bar{2}} - R_1R_{22\bar{2}})(R_1R_{1\bar{1}2} - R_2R_{11\bar{1}})}{(R_{11\bar{1}}R_{22\bar{2}} - R_{1\bar{1}2}R_{12\bar{2}})^2}}$$

Then, the solution N_3 is stable if $tr < 0$ and $\det > 0$ hold. Here $tr = (a'+b')$, $\det = (a'b'-c'd')$. Specifically, a pair of purely imaginary eigenvalues appears in Eq. (31) when the condition of $tr = 0$ is satisfied. In this case, the solution N_3 loses its stability at the critical line

$$L_5: \; R_1(R_{1\bar{1}2}R_{22\bar{2}} - R_{11\bar{1}}R_{22\bar{2}}) + R_2(R_{11\bar{1}}R_{12\bar{2}} - R_{11\bar{1}}R_{22\bar{2}}) = 0 \tag{32}$$

and a three-dimensional torus solution can be bifurcated from the quasi-periodic solution N_3 [35]. For this case, the stability conditions and the corresponding existence conditions for each solution N_i, $i = 0, 1, 2, 3$ should be considered simultaneously. In the next subsection, the unfolding results for the marked double Hopf bifurcation points in Figs. 4(b-e) will be presented.

5.2 Numerical examples with different delays

The double Hopf bifurcation point H_1 with $\tau = 0.5$ in Figs. 4(b) is located at $(c_0, k_0) = (0.294678, 0.397493)$ and the corresponding frequencies are calculated as

$\omega_1 \approx 0.547704$ and $\omega_2 \approx 1.174274$. By implementing the MMS, the deterministic amplitude equations (26) for the bifurcation point H_1 are given by

$$\begin{aligned}\dot{\rho}_1 &= (-0.589831c_\varepsilon - 0.514915k_\varepsilon)\rho_1 - 1.369149\rho_1^3 - 1.191842\rho_1\rho_2^2 \\ \dot{\rho}_2 &= (-0.528117c_\varepsilon - 0.153181k_\varepsilon)\rho_2 + 0.474446\rho_1^2\rho_2 + 0.077205\rho_2^3\end{aligned} \tag{33}$$

Further, by considering the existence conditions (C0)-(C3) and the stability conditions (S0)-(S3) of the possible solutions in Eq. (33), the bifurcating response near bifurcation point H_1 is shown in Fig. 6, where the bifurcation lines $L_i, i = 1, 2, 3, 4, 5$ are calculated as

$$\begin{aligned}&L_1 : k_\varepsilon = -1.145492c_\varepsilon,\ L_2 : k_\varepsilon = -3.447674c_\varepsilon,\ L_3 : k_\varepsilon = -2.208932c_\varepsilon, \\ &L_4 : k_\varepsilon = -3.036013c_\varepsilon,\ L_5 : k_\varepsilon = -2.950603c_\varepsilon.\end{aligned} \tag{34}$$

In this case, a secondary bifurcation occurs. The solution N_3 loses its stability at bifurcation line L_5 and a three-dimensional torus solution arises. It should be mentioned that the existence region of the three-dimensional torus solution in the $(c_\varepsilon, k_\varepsilon)$ plane is not specifically delineated for its narrow characteristic. To briefly describe the dynamic response presented in Fig. 6, a clockwise direction from regions I to VII is selected. In region I, only trivial equilibrium N_0 exists, which is a saddle point for Eq. (33). By crossing the bifurcation line L_2 to region II, an unstable periodic solution N_2 is generated from the Hopf bifurcation of trivial equilibrium N_0, and N_0 becomes stable. On passing through the bifurcation line L_1 to region III, a stable periodic solution N_1 appears and the trivial equilibrium N_0 becomes a saddle point again. By changing the parameters into region IV, system (6) has a stable quasi-periodic solution which is related to the stable focus in Eq. (33), and N_1 becomes a saddle point. When the parameters are changed across line L_5 into region V, the quasi-periodic solution N_3 loses its stability and a three-dimensional torus

solution emerges. Further, after colliding with the periodic solution N_2 at line L_4, the unstable quasi-periodic solution N_3 disappears in region VI. As the parameters are changed across line L_2 into region VII, the periodic solution N_2 collides with the trivial equilibrium N_0 and disappears, and N_0 changes from a saddle point to an unstable node. Finally, the periodic solution N_1 collides with N_0 at line L_1 and disappears in region I, and N_0 returns to the saddle.

To illustrate the theoretically predicted stable response in Fig. 6, some phase portraits corresponding to regions II, III and IV are shown in Figs. 7(a-d). The stable equilibrium corresponding to region II is displayed in Fig. 7(a), the stable periodic solution corresponding to region III is illustrated in Fig. 7(b) and the stable quasi-periodic solution corresponding to region IV is demonstrated in Figs. 7(c-d). This indicates that the theoretical analysis is well verified by the numerical simulations.

When the delay is increased to $\tau = 1$, the double bifurcation point H_2 appearing in Fig. 4(c) is located at $(c_0, k_0) = (0.591407, 0.143178)$. At the bifurcation point, the frequencies are calculated as $\omega_1 \approx 0.502343$ and $\omega_2 \approx 1.108387$. The corresponding amplitude equations at this point are given by

$$\begin{aligned} \dot{\rho}_1 &= (-0.285825\, c_\varepsilon - 0.736909\, k_\varepsilon)\rho_1 - 1.260580\rho_1^3 - 2.494655\rho_1\rho_2^2 \\ \dot{\rho}_2 &= (-0.418125\, c_\varepsilon - 0.453216 k_\varepsilon)\rho_2 - 0.924591\rho_1^2\rho_2 - 0.117106\rho_2^3 \end{aligned} \tag{35}$$

Accordingly, the dynamic behaviors near the bifurcation point H_2 is shown in Fig. 8. Only the stable equilibrium N_0 exists in region I. By crossing the line L_1 into region II, a stable periodic solution N_1 arises and N_0 becomes unstable. Upon passing the line L_2 into region III, a new and unstable periodic solution N_2 appears.

When the parameters are located in region IV, an unstable quasi-periodic solution N_3 emerges and two stable periodic solutions, i.e., N_1 and N_2 coexist. The unstable quasi-periodic solution N_3 collides with the stable periodic solution N_1 at line L_3, resulting in the disappearance of quasi-periodic solution N_3 and an unstable periodic solution N_1. The periodic solution N_1 further disappears in region VI by colliding with the equilibrium N_0. Finally, the stable periodic solution N_2 collides with equilibrium N_0 at line L_2 and disappears in region I.

To verify the theoretical results presented in Fig. 8, six groups of perturbation parameters corresponding to regions I-VI, are chosen to obtain the numerical solutions, which are displayed in Figs. 9(a-f). It is evident that the numerical simulations and the theoretical analyses are in good agreement.

As the time delay is sequentially varied to $\tau = 1.5$ and $\tau = 2$, three new double bifurcation points $H_i, i = 3, 4, 5$, appear on the stability boundaries of equilibrium E_1, which correspond to Fig. 4(d) and Fig. 4(e), respectively. By performing the unfolding analysis at these three bifurcation points, it is found that the system responses near points H_3 and H_4 are topologically equivalent to the case shown in Fig. 8. However, the unfolding at the bifurcation point H_5 is different from the aforementioned cases shown in Fig. 6 and Fig. 8. At the bifurcation point H_5, the corresponding frequencies are obtained as $\omega_1 \approx 0.610585$ and $\omega_2 \approx 1.152642$, and the deterministic amplitude equations (26) are:

$$\begin{aligned} \dot{\rho}_1 &= (-0.504865\, c_\varepsilon - 0.044023\, k_\varepsilon)\rho_1 - 0.074100\rho_1^3 - 0.239390\rho_1\rho_2^2 \\ \dot{\rho}_2 &= (-0.318728\, c_\varepsilon - 0.015836 k_\varepsilon)\rho_2 + 0.535384\rho_1^2\rho_2 - 0.042133\rho_2^3 \end{aligned} \tag{36}$$

Accordingly, the system response near the bifurcation point H_5 is presented in Fig.

10. In region I, only stable equilibrium N_0 exists. By moving across line L_1 into region II, a stable periodic solution N_1 appears and N_0 becomes unstable. In region III, a stable quasi-periodic solution N_3 is generated from the Hopf bifurcation of periodic solution N_1 and the periodic solution N_1 loses its stability. On entering into region IV by crossing line L_2, a new and unstable periodic solution N_2 arises. The stable quasi-periodic solution N_3 collides with the unstable periodic solution N_2 at line L_4 and disappears in region V. Meanwhile, the periodic solution N_2 becomes stable. The unstable periodic solution N_1 disappears in region VI. After that, the stable periodic solution N_2 collides with the unstable equilibrium N_0 at line L_2, and the equilibrium N_0 regains its stability in region I.

To demonstrate the theoretically predicted results shown in Fig. 10, six groups of perturbation parameters corresponding to regions I-VI are chosen and the numerical solutions are presented in Figs. 11(a-h). A good agreement is achieved between the theoretical predictions and numerical simulations.

5.3 Other possible co-dimension two bifurcations

According to the above analysis, there are two types of stability boundaries, i.e., the stability boundary with zero eigenvalue marked by the black solid lines in Figs. 3-4 and the stability boundary with purely imaginary eigenvalue marked by the blue solid lines in Figs. 3-4. In addition to the observed double Hopf bifurcation, the other possible co-dimensional two bifurcations, i.e., the double zero bifurcation and the zero-Hopf bifurcation will be discussed in the subsection by analyzing the characteristic equations.

First, the existence of double zero bifurcation is considered for the system. Based on the characteristic equations (21) and (23) for equilibriums E_0 and E_1, only one

curve with $ck=1$ satisfied is calculated as the curve of zero eigenvalue and the time delay does not change the curve of zero eigenvalue. Therefore, the double zero bifurcation is impossible for the two equilibria E_0 and E_1.

Secondly, the existence of zero-Hopf bifurcation is studied. For equilibrium E_0, two families of characteristic Eq. (21) should be satisfied if there exists a zero-Hopf bifurcation point in the case, which are given by

$$\begin{cases} D(0,\tau)=0, & \omega=0 \\ D(i\omega,\tau)=0, & \omega\neq 0 \end{cases} \tag{37}$$

The corresponding frequency equations (22) can then be obtained as

$$\begin{cases} f_0(c,k,\omega)\big|_{\omega=0} = ck-1=0, \\ f_1(c,k,\omega)\big|_{\omega\neq 0} = -\omega^6+(3c^2+9ck+3k^2)\omega^4+\dfrac{\sin(3\omega\tau)}{c^3}\omega^3+(\dfrac{3\cos(3\omega\tau)}{c^2}-3c^3k \\ \qquad -9c^2k^2-3ck^3)\omega^2-\dfrac{3\sin(3\omega\tau)}{c}\omega+c^3k^3-\cos(3\omega\tau)=0, \\ f_2(c,k,\omega)\big|_{\omega\neq 0} = (3c+3k)\omega^5+(\dfrac{\cos(3\omega\tau)}{c^3}-c^3-9c^2k-9ck^2-k^3)\omega^3 \\ \qquad -\dfrac{3\sin(3\omega\tau)}{c^2}\omega^2+(3c^3k^2+3c^2k^3-\dfrac{3\cos(3\omega\tau)}{c})\omega+\sin(3\omega\tau)=0. \end{cases} \tag{38}$$

Substituting the first equation f_0 in Eq. (38) into the last two equations and considering the condition of $\sin^2(3\omega\tau)+\cos^2(3\omega\tau)=1$, yields the following frequency equation

$$\begin{aligned} f_3(c,\omega)\big|_{\omega\neq 0} = {} & \omega^{12}+(\frac{3}{c^2}+3c^2)\omega^{10}+(\frac{3}{c^4}+3c^4+9)\omega^8+(\frac{9}{c^2}+9c^2+c^6)\omega^6 \\ & +(3c^4+9)\omega^4+3c^2\omega^2=0 \end{aligned} \tag{39}$$

Therefore, there exists a zero-Hopf bifurcation point for equilibrium E_0 if Eq. (39) has the solution (c,ω) with $\omega\neq 0$. By considering the existence condition of equilibrium E_0, i.e., $c\neq 0$, it can be seen that no such solution (c,ω) can be detected in Eq. (39) for the reason of $f_3>0$ with $c\neq 0$ and $\omega\neq 0$. Thus, no

zero-Hopf bifurcation point could exist for equilibrium E_0. In addition, it should be mentioned that the time delay has no impact on the zero-Hopf bifurcation, since no solution (c, ω) is found from Eq. (39) and the corresponding delay for the zero-Hopf bifurcation does not exist. For equilibrium E_1, the two families of characteristic equations and frequency equations corresponding to the zero-Hopf bifurcation are identical to the expressions for equilibrium E_0 in Eq. (37) and Eq. (38), since equilibrium E_0 and equilibrium E_1 collide as one point when the condition of $\lambda = 0$, i.e., $ck = 1$ is considered. Thus, there is no zero-Hopf bifurcation for equilibrium E_1 either, and this situation is not affected by changing the time delay.

In summary, the other possible co-dimensional two bifurcations, i.e., the double zero and zero-Hopf bifurcations, would not occur in the system.

6 Delay-induced chaotic motions and new coexistence patterns of multi-stability in the three-disk dynamo system

It has been demonstrated that the effect of time delay on the local dynamics of the three-disk dynamo system cannot be neglected, while the effect on the dynamic behavior of the system corresponding to the parameter regions of unstable equilibrium is unknown. In order to study the system behaviors in the parameter regions where the equilibrium is unstable and examine the influence of time delay, a group of fixed system parameters (c, k) is chosen to analyze the evolution process of system behaviors with the time delay considered as the single bifurcation parameter. The system parameters are chosen as $(c, k) = (0.4, 0.2)$, where three equilibria $E_i, i = 0, 1, 2$ are all unstable in the case. For a better visualization on the evolution

process of system behaviors with different initial conditions, the numerical simulations conducted in the section are directed to the original system (2). Moreover, the simulated results of dynamic responses near equilibrium E_0 with the fixed initial condition $(0.1, 0, 0, 2.5, 2.5, 2.5)$, equilibrium E_1 with the fixed initial condition $(1.06, 0.96, 0.96, 0.2, 0.2, 0.2)$, and near equilibrium E_2 with the fixed initial condition $(-1.06, -0.96, -0.96, 0.2, 0.2, 0.2)$, are marked by red, blue and black colors, respectively. To begin with, define the Poincare section as

$$\Pi = \{(x_1, x_2, x_3, y_2, y_3) \in R^5 \mid y_1 = 0, \ \dot{y}_1 > 0\} \tag{40}$$

First, the system response is discussed for the case of $\tau = 0$. Two stable periodic orbits generated from the Hopf bifurcation of equilibria $E_{1,2}$ are shown in Fig. 12. To further illustrate the global continuation of the bifurcated periodic orbits with respect to the time delay, the bifurcation diagrams with above-mentioned three initial conditions are plotted in Fig. 13(a). Meanwhile, the largest Lyapunov exponent LLE is calculated to distinguish different attractors. The corresponding three curves of largest Lyapunov exponents are presented in Fig. 13(b). It is noted that the curves of largest Lyapunov exponents marked by the blue solid line and the black solid line are overlapped. As shown in Fig. 13, there exist two period-1 attractors when the time delay is small. As the delay increases, a chaotic attractor appears and coexists with the two period-1 attractors, as shown in Figs. 14(a-b). Further, the pair of period-1 attractors disappear and only the chaotic attractor exists in the system for a large range of time delay. The coexistence of two quasi-periodic attractors is then observed in the system as illustrated in Figs. 14(c-d). When the value of time delay is gradually increased, the pair of quasi-periodic attractors disappear and the chaotic attractor appears again. Finally, the two quasi-periodic attractors coexisting with a chaotic

attractor are observed in the system, as shown in Figs. 14(e-f). According to the above continuation analysis, many new delay-induced nonlinear behaviors are observed in the three-disk dynamo system with certain system parameters, including diverse coexistence patterns of multiple attractors and the chaotic motions.

7 Conclusions

By investigating and comparing the dynamic behaviors of a coupled three-disk dynamo system with and without time delay, it has clearly demonstrated that the time delay could significantly affect the dynamic behaviors of the three-disk dynamo system. The main conclusions are listed below:

1. For the equilibrium E_0, the corresponding local stability and bifurcation remain unchanged as the time delay varies from 0 to 2. Only the pitchfork bifurcation occurs on the stability boundary of the equilibrium;

2. For the equilibrium E_1, the time delay can influence the local stability and bifurcation of the equilibrium. Compared to the non-delay case, more complicated stability boundaries are caused by the time delay. Meanwhile, the size and shape of the stability region of the equilibrium are changed and the phenomenon of stability switches is observed in certain parameter regions. As for the bifurcations occurring on the stability boundaries, two types of co-dimension one bifurcations, i.e., the pitchfork and generic Hopf bifurcations, are found for both cases of $\tau = 0$ and $\tau > 0$.

3. Due to the appearance of the intersection points on the stability boundaries of equilibrium E_1, a novel co-dimension two bifurcation, i.e., double Hopf bifurcations, is induced by time delay in the three-disk dynamo system. By performing the bifurcation analyses for all intersection points, three different topological structures of unfolding are found with certain time delays. Accordingly, the new steady-state

responses, including the two-dimensional torus, three-dimensional torus and the coexistence of multiple attractors, can arise in the delayed dynamo system. Notably, a variety of coexistence patterns of multiple attractors can be observed in the small neighborhood of double Hopf bifurcation points, including the coexistence of two stable periodic orbits, the coexistence of four stable periodic orbits, and the coexistence of two stable quasi-periodic orbits, due to the symmetry property.

4. On the stability boundaries of the system, i.e., the boundaries with zero eigenvalue and purely imaginary eigenvalues, two types of co-dimensional two bifurcations, the double zero and zero-Hopf bifurcations, would be expected to appear in some intersection points. However, by detecting the existence of characteristic eigenvalues corresponding to these two types of bifurcations, it is theoretically proved that the double zero and zero-Hopf bifurcations cannot arise in the system and the time delay does not have any influence on the existence of these two bifurcations.

5. In addition to the local dynamics analyses, the dynamic responses occurring in other two-parameter regions corresponding to the unstable equilibria are also discussed with the aid of numerical techniques. Many new nonlinear phenomena, e.g., the chaotic motions, two period-1 attractors coexisting with a chaotic attractor, and two quasi-periodic attractors coexisting with a chaotic attractor, can be induced in the three-disk dynamo system by changing the time delay only.

In short, the necessity of considering time delay effect in a three-disk dynamo system has been confirmed in this study. Compared to the three-disk dynamo system in the absence of time delay, more rich and complex nonlinear behaviors are observed in the delayed three-disk dynamo system. In view of this, it is hoped that the present work could provide an useful reference on the study of geodynamo for the possible similarity in the coupling and behaviour.

Finally, although the time delay is demonstrated to have a substantial effect on the dynamic behavior under certain system parameters belonging to the parameter regions of unstable equilibria, the global behaviors in the whole two-parameter plane are yet to be fully investigated. In order to develop an in-depth understanding of the three-disk dynamo dynamics, the two-parameter global dynamics analysis will be conducted in the future.

Acknowledgments

The authors would like to acknowledge the financial supports from the Key Program of National Natural Science Foundation of China (No. 11832009), the National Natural Science Foundation of China (No. 11672104), and the Applied Basic Research Program of Shanxi Province of China (No. 201801D121021).

References

[1] E. Bullard, The stability of a homopolar dynamo, Math. Proc. Camb. Philos. Soc. 51(4) (1955) 744–760.

[2] T. Rikitake, Oscillations of a system of disk dynamos, Math. Proc. Camb. Philos. Soc. 54(1) (1958) 89-105.

[3] A.E. Cook, Two disc dynamos with viscous friction and time delay, Math. Proc. Camb. Philos. Soc. 71(1) (1972) 135-153.

[4] K.A. Robbins, A new approach to subcritical instability and turbulent transitions in a simple dynamo, Math. Proc. Camb. Philos. Soc. 82(2) (1977) 309-325.

[5] H.K. Moffatt, A self-consistent treatment of simple dynamo systems, Geophys. Astrophys. Fluid Dyn. 14(1) (1979) 147-166.

[6] R. Hide, The nonlinear differential equations governing a hierarchy of

self-exciting coupled faraday-disk homopolar dynamos, Phys. Earth Planet. Inter. 103(3-4) (1997) 0-291.

[7] I.M. Moroz, On the behavior of a self-exciting faraday disk homopolar dynamo with a variable nonlinear series motor, Int. J. Bifurcation Chaos 12(10) (2002) 2123-2135.

[8] Z. Wei, B. Zhu, J. Yang, M. Perc, M. Slavinec, Bifurcation analysis of two disc dynamos with viscous friction and multiple time delays, Appl. Math. Comput. 347 (2019) 265-281.

[9] J. Llibre, M. Messias, Global dynamics of the Rikitake system, Physica D 238(3) (2009) 241-252.

[10] T. Miura, T. Kai, Chaotic behaviours of a system of three disk dynamos, Phys. Lett. A 101(9) (1984) 450-454.

[11] P. Muthukumar, P. Balasubramaniam, K. Ratnavelu, Detecting chaos in a system of four disk dynamos and its control, Nonlinear Dyn. 83(4) (2015) 1-8.

[12] V. Vembarasan, P. Balasubramaniam, Chaotic synchronization of Rikitake system based on T-S fuzzy control techniques, Nonlinear Dyn. 74(1-2) (2013) 31-44.

[13] Z. Wei, I. Moroz, J.C. Sprott, A. Akgul, W. Zhang, Hidden hyperchaos and electronic circuit application in a 5D self-exciting homopolar disc dynamo, Chaos 27(3) (2017) 033101.

[14] Z. Wei, A. Akgul, U.E. Kocamaz, I. Moroz, W. Zhang, Control, electronic circuit application and fractional-order analysis of hidden chaotic attractors in the self-exciting homopolar disc dynamo, Chaos Solitons Fractals 111 (2018) 157-168.

[15] H. Logemann, R. Rebarber, The effect of small time-delays on the closed-loop stability of boundary control systems, Math. Control Signal Syst. 9(2) (1996) 123-151.

[16] S. Deng, J. Ji, G. Wen, H. Xu, Delay-induced novel dynamics in a hexagonal centrifugal governor system, Int. J. Non-Linear Mech. 121 (2020) 103465.

[17] H. Lu, Z. He, Chaotic behavior in first-order autonomous continuous-time systems with delay, IEEE Trans. Circuits Syst. I-Regul. Pap. 43(8) (1996) 700-702.

[18] X. Sun, J. Xu, X. Jing, L. Cheng, Beneficial performance of a quasi-zero-stiffness vibration isolator with time-delayed active control, Int. J. Mech. Sci. 82 (2014) 32-40.

[19] Y.X. Sun, J. Xu, Experiments and Analysis for a Controlled Mechanical Absorber Considering Delay Effect, J. Sound Vibr. 339 (2015) 25–37.

[20] X. Zhang, J. Xu, J. Ji, Modelling and tuning for a time-delayed vibration absorber with friction, J. Sound Vibr. 424 (2018) 137-157.

[21] Z.H. Wang, H.Y. Hu, Q. Xu, G. Stepan, Effect of delay combinations on stability and Hopf bifurcation of an oscillator with acceleration-derivative feedback, Int. J. Non-Linear Mech. 94 (2017) 392–399.

[22] G. Zhuang, S. Xu, J. Xia, Q. Ma, Z. Zhang, Non-fragile delay feedback control for neutral stochastic Markovian jump systems with time-varying delays, Appl. Math. Comput. 355 (2019) 21–32..

[23] S. Deng, J. Ji, S. Yin, G. Wen, Multistability in the Centrifugal Governor System Under a Time-Delay Control Strategy, J. Comput. Nonlinear Dyn. 14(11) (2019).

[24] J.K. Hale, Theory of Functional Differential Equations, SpringerVerlag, New York, 2003.

[25] S.J. Guo, J. Wu, Bifurcation Theory of Functional Differential Equations, Springer, New York, 2013.

[26] T.H. Scholl, L. Gröll, V. Hagenmeyer, Time delay in the swing equation: A variety of bifurcations, Chaos 29(12) (2019) 123118.

[27] J. Cantisán, M. Coccolo, J.M. Seoane, M.A.F. Sanjuán, Delay-Induced Resonance in the Time-Delayed Duffing Oscillator, Int. J. Bifurcation Chaos 30(3) (2020) 2030007.

[28] L. Pei, Y. Chen, S. Wang, Complicated oscillations and non-resonant double Hopf bifurcation of multiple feedback delayed control system of the gut microbiota, Nonlinear Anal.-Real World Appl. 54 (2020) 103091.

[29] C.H. Zhang, Y. He, Multiple stability switches and Hopf bifurcations induced by the delay in a Lengyel-Epstein chemical reaction system, Appl. Math. Comput. 378 (2020) 125201.

[30] S. Khajanchi, J.J. Nieto, Mathematical modeling of tumor-immune competitive system, considering the role of time delay, Appl. Math. Comput. 340 (2019) 180–205.

[31] A.H. Nayfeh, Order reduction of retarded nonlinear systems-the method of multiple scales versus center-manifold reduction, Nonlinear Dyn. 51(4) (2008) 483-500.

[32] A. Luongo, A. Paolone, A.D. Egidio, Multiple timescales analysis for 1:2 and 1:3 resonant hopf bifurcations, Nonlinear Dyn. 34(3-4) (2003) 269-291.

[33] G. Stépán, Retarded dynamical systems: stability and characteristic functions, Longman Scientif. and Techn, Harlow, 1989.

[34] Y. A. Kuznetsov, Elements of Applied Bifurcation Theory, Springer, New York, 2004.

[35] P. Yu, Analysis on double Hopf bifurcation using computer algebra with the aid of multiple scales, Nonlinear Dyn. 27(1) (2002) 19-53.

List of Figure Captions

Fig. 1 Mechanical model of the three-disk dynamo.

Fig. 2 The existence regions of equilibria of system (2) in the two-parameter (c,k) plane.

Fig. 3 Linear stabilities and nonlinear dynamic responses of the equilibria with $\tau = 0$. (a) Stability region of equilibrium E_0 and the point PB with $(c,k) = (1,1)$ denotes the pitchfork bifurcation point. (b) Pitchfork bifurcation of equilibrium E_0 near PB. (c) Stability region of equilibrium E_1 and the point CH with $(c,k) = (0.5, 0.274944)$ denotes the generic Hopf bifurcation point. (d) Generic Hopf bifurcation of equilibrium E_1 near CH.

Fig. 4 Linear stabilities and nonlinear dynamic responses of the equilibria with $\tau > 0$, where the black stability boundary curves represent the pitchfork bifurcations and the blue stability boundary curves represent the generic Hopf bifurcations. The asterisks '*' indicate the double Hopf bifurcation points, where H_1 corresponds to $(c,k) = (0.294678, 0.397493)$, H_2 corresponds to $(c,k) = (0.591407, 0.143178)$, H_3 corresponds to $(c,k) = (0.860436, 0.050393)$, H_4 corresponds to $(c,k) = (1.028187, 0.021681)$ and H_5 corresponds to $(c,k) = (0.095406, 1.517501)$. (a) Equilibrium E_0 with $\tau = 0.5,\ 1,\ 1.5,\ 2$. (b) Equilibrium E_1 with $\tau = 0.5$. (c) Equilibrium E_1 with $\tau = 1$. (d) Equilibrium E_1 with $\tau = 1.5$. (e) Equilibrium E_1 with $\tau = 2$.

Fig. 5 The stability switch with the fixed system parameters $(c,k) = (0.6, 0.15)$ and the initial condition $(0.01, 0, 0, 0, 0, 0)$.

Fig. 6 The unfolding of double Hopf bifurcation point H_1 with $\tau = 0.5$.

Fig. 7 Numerical simulations of regions II, III and IV in Fig. 6. (a) The stable equilibrium with the perturbation parameters $(c_\varepsilon, k_\varepsilon) = (0.01, 0.01)$ and the initial

condition $(0.006,0,0,0,0,0)$, where the red dot represents the simulated end point. (b) The stable periodic orbit with the perturbation parameters $(c_\varepsilon,k_\varepsilon)=(0.01,-0.015)$ and the initial condition $(0.1,0,0,0,0,0)$. (c-d) The quasi-periodic orbit with perturbation parameters $(c_\varepsilon,k_\varepsilon)=(0.01,-0.025)$ and the initial condition $(0.3,0,0,0,0,0)$.

Fig. 8 The unfolding of double Hopf bifurcation point H_2 with $\tau=1$.

Fig. 9 Numerical simulations of regions I-VI in Fig. 8, where the periodic orbits marked by the blue solid lines and the red solid lines correspond to the motions with frequencies ω_1 and ω_2, respectively. (a) The stable equilibrium with perturbation parameters $(c_\varepsilon,k_\varepsilon)=(0.01,0.01)$ and the initial condition $(0.006,0,0,0,0,0)$, where the red dot denotes the simulated end point. (b) The stable periodic orbit with perturbation parameters $(c_\varepsilon,k_\varepsilon)=(0.015,-0.01)$ and the initial condition $(0.1,0,0,0,0,0)$. (c) The stable periodic orbit with perturbation parameters $(c_\varepsilon,k_\varepsilon)=(0.01,-0.0095)$ and the initial condition $(0.1,0,0,0,0,0)$. (d) The stable periodic orbits with perturbation parameters $(c_\varepsilon,k_\varepsilon)=(0,-0.01)$, where the blue solid line corresponds to the initial condition $(-0.07,-0.07,0.14,-0.09,0.05,0.05)$ and the red solid line corresponds to the initial condition $(0.1,0,0,0,0,0)$. (e) The stable periodic orbit with the perturbation parameters $(c_\varepsilon,k_\varepsilon)=(-0.01,-0.01)$ and the initial condition $(0.54,0,0,0,0,0)$. (f) The stable periodic orbit with perturbation parameters $(c_\varepsilon,k_\varepsilon)=(-0.015,0.01)$ and the initial condition $(0.5,0,0,0,0,0)$.

Fig. 10 The unfolding of double Hopf bifurcation point H_5 with $\tau=2$.

Fig. 11 Numerical simulations of regions I-VI in Fig. 10, where the periodic orbits marked by the blue solid lines and the red solid lines correspond to the motions with

frequencies ω_1 and ω_2, respectively. (a) The stable equilibrium with perturbation parameters $(c_\varepsilon, k_\varepsilon) = (0, 0.01)$ and the initial condition $(0.001, 0, 0, 0, 0, 0)$, where the red dot represents the simulated end point. (b) The stable periodic orbit with perturbation parameters $(c_\varepsilon, k_\varepsilon) = (0.004, -0.046)$ and the initial condition $(0.2, 0, 0, 0, 0, 0)$. (c-d) The quasi-periodic torus with perturbation parameters $(c_\varepsilon, k_\varepsilon) = (0.002, -0.03)$ and the initial condition $(0.2, 0.3, 0.3, 0.2, 0.2, 0.2)$. (e-f) The quasi-periodic torus with perturbation parameters $(c_\varepsilon, k_\varepsilon) = (0.0015, -0.035)$ and the initial condition $(0.4, 0, 0, 0, 0, 0)$. (g) The stable periodic orbit with perturbation parameters $(c_\varepsilon, k_\varepsilon) = (0, -0.01)$ and the initial condition $(0.4, 0, 0, 0, 0, 0)$. (h) The stable periodic orbit with perturbation parameters $(c_\varepsilon, k_\varepsilon) = (-0.003, 0.04)$ and the initial condition $(0.4, 0, 0, 0, 0, 0)$.

Fig. 12 Phase portraits of system (2) with the fixed system parameters $(c, k) = (0.4, 0.2)$ and time delay $\tau = 0$, where the steady-state responses marked by blue and black solid lines are obtained from the initial conditions $(1.06, 0.96, 0.96, 0.2, 0.2, 0.2)$ and $(-1.06, -0.96, -0.96, 0.2, 0.2, 0.2)$, respectively.

Fig. 13 Numerical simulations of system (2) with the fixed system parameters $(c, k) = (0.4, 0.2)$ and bifurcation parameter τ, where the steady-state responses marked by red, blue and black solid lines are obtained from the initial conditions $(0.1, 0, 0, 2.5, 2.5, 2.5)$, $(1.06, 0.96, 0.96, 0.2, 0.2, 0.2)$ and $(-1.06, -0.96, -0.96, 0.2, 0.2, 0.2)$, respectively. (a) Bifurcation diagram. (b) The largest Lyapunov exponents.

Fig. 14 Numerical simulations of system (2) with the fixed system parameters $(c, k) = (0.4, 0.2)$ and time delay $\tau > 0$, where the different steady-state responses

are obtained from different initial conditions and the descriptions can be found in Fig. 13. (a) Phase portrait with $\tau = 0.55$. (b) Poincare section with $\tau = 0.55$. (c) Phase portrait with $\tau = 1.68$. (d) Poincare section with $\tau = 1.68$. (e) Phase portrait with $\tau = 1.9$. (f) Poincare section with $\tau = 1.9$.

Figures

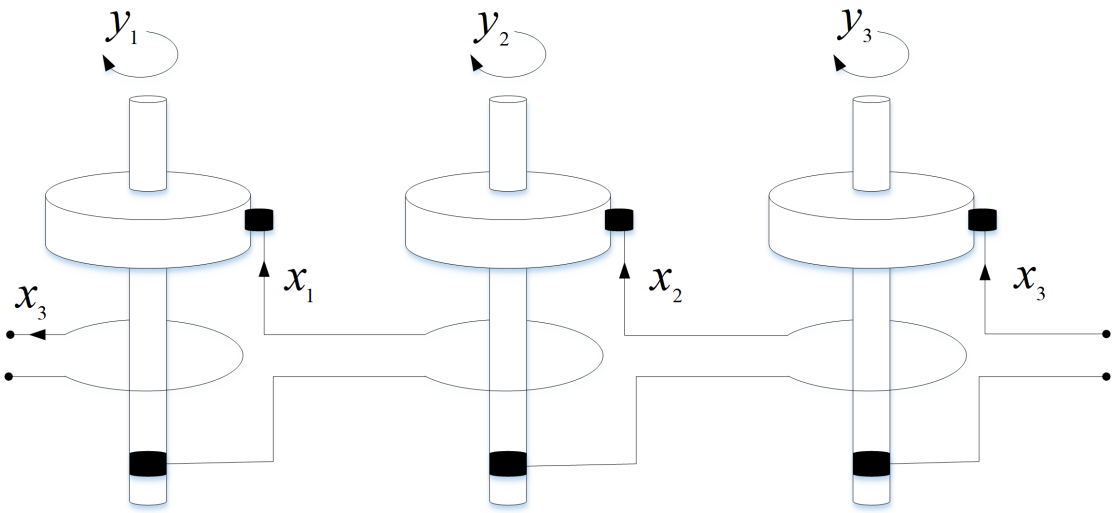

Fig. 1

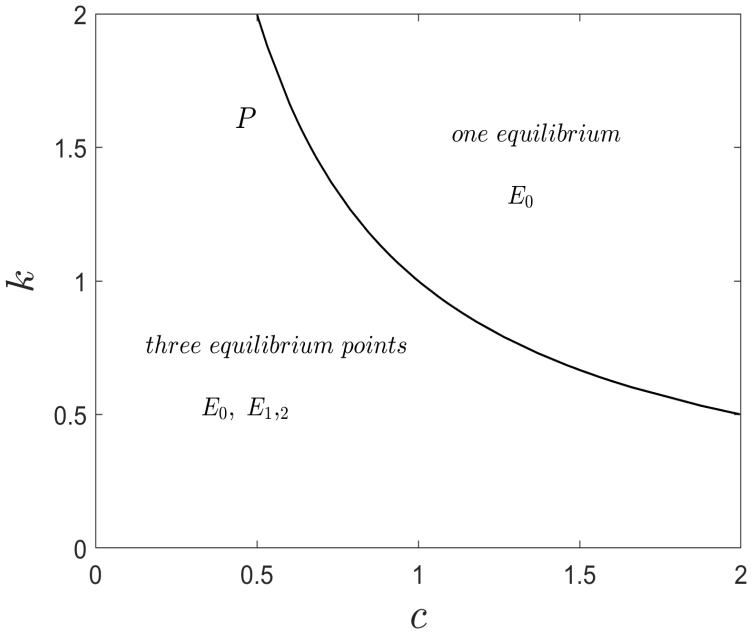
P
one equilibrium
E_0
three equilibrium points
$E_0,\ E_{1,2}$
k
c
0
0.5
1
1.5
2

Fig. 2

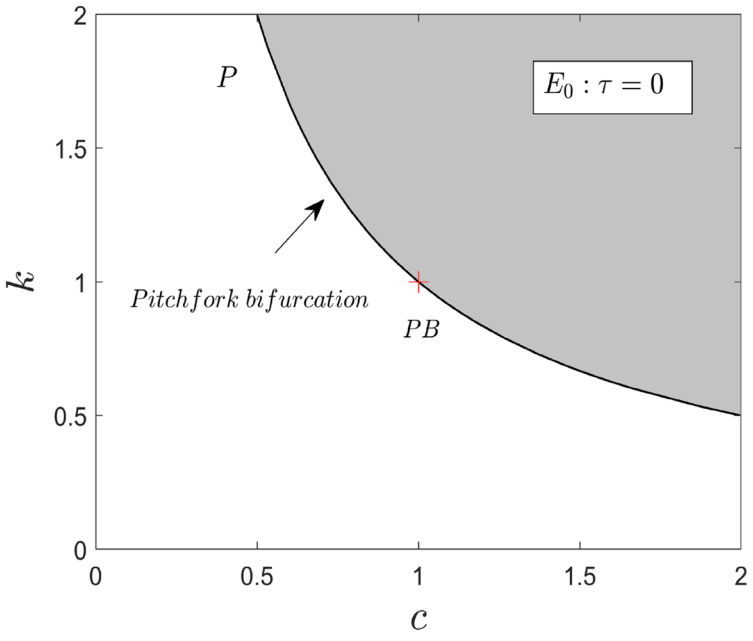
P
$E_0 : \tau = 0$
Pitchfork bifurcation
PB
k
c
0
0.5
1
1.5
2

Fig. 3(a)

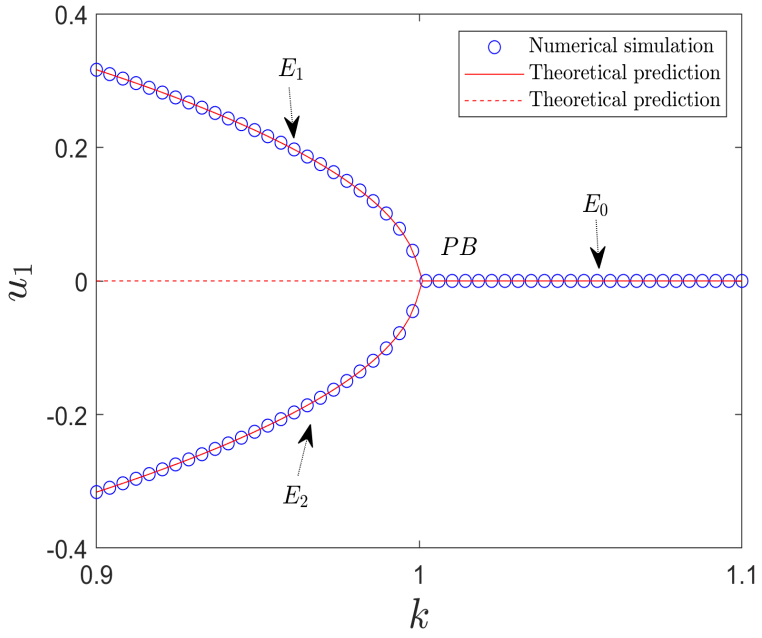
Numerical simulation
Theoretical prediction
Theoretical prediction
E_1
E_0
PB
E_2
u_1
k
0.4
0.2
0
-0.2
-0.4
0.9
1
1.1

Fig. 3(b)

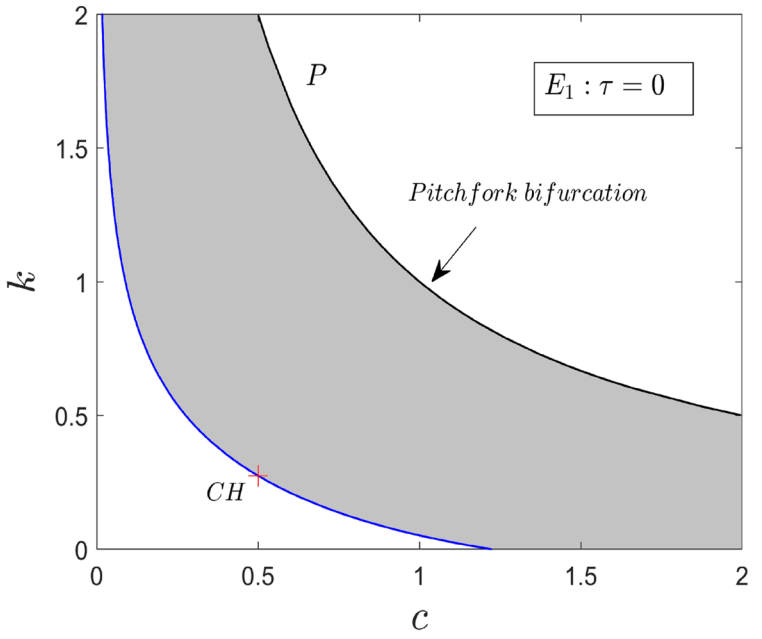
P
$E_1 : \tau = 0$
$Pitchfork\ bifurcation$
CH
k
c
2
1.5
1
0.5
0
0
0.5
1
1.5
2

Fig. 3(c)

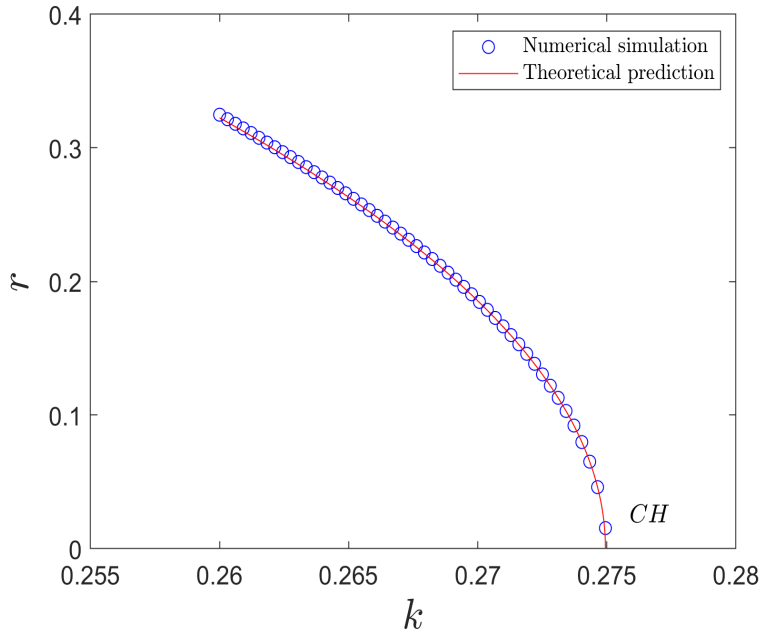
Numerical simulation
Theoretical prediction
CH
r
k
0.4
0.3
0.2
0.1
0
0.255
0.26
0.265
0.27
0.275
0.28

Fig. 3(d)

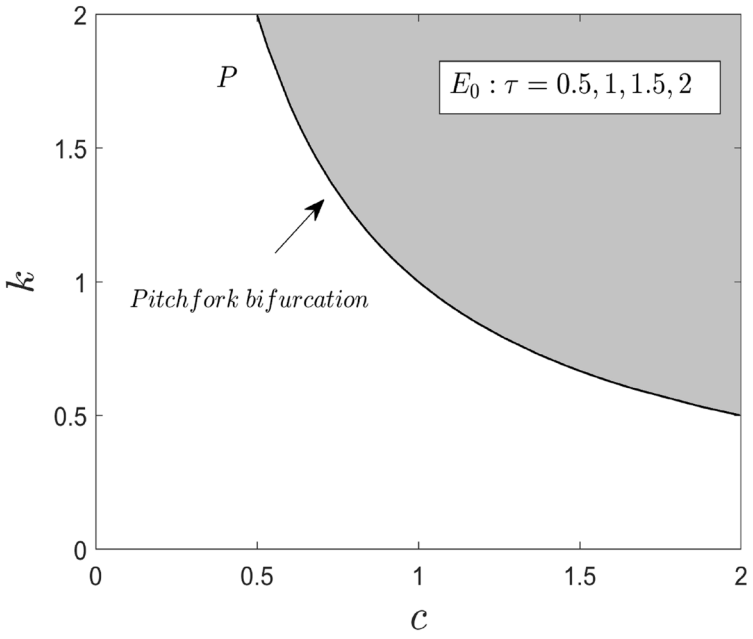
P
$E_0 : \tau = 0.5, 1, 1.5, 2$
Pitchfork bifurcation
k
c
2
1.5
1
0.5
0
0
0.5
1
1.5
2

Fig. 4(a)

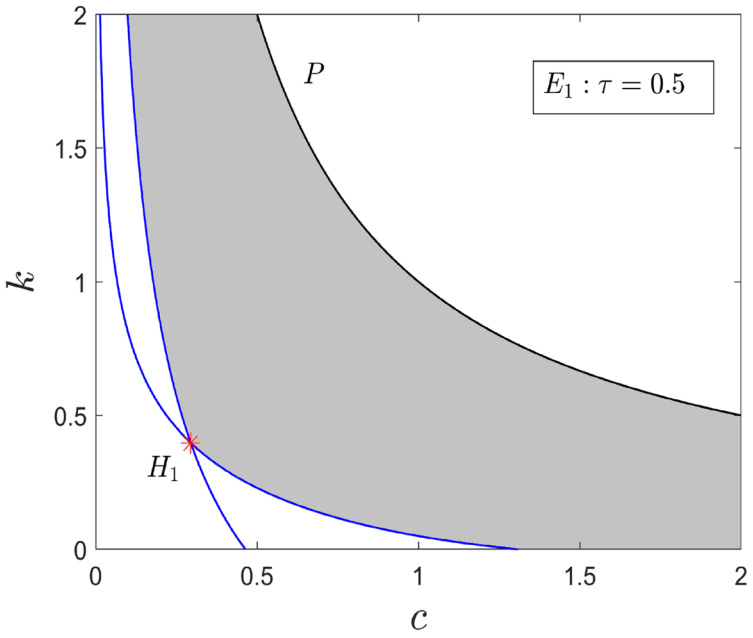

Fig. 4(b)

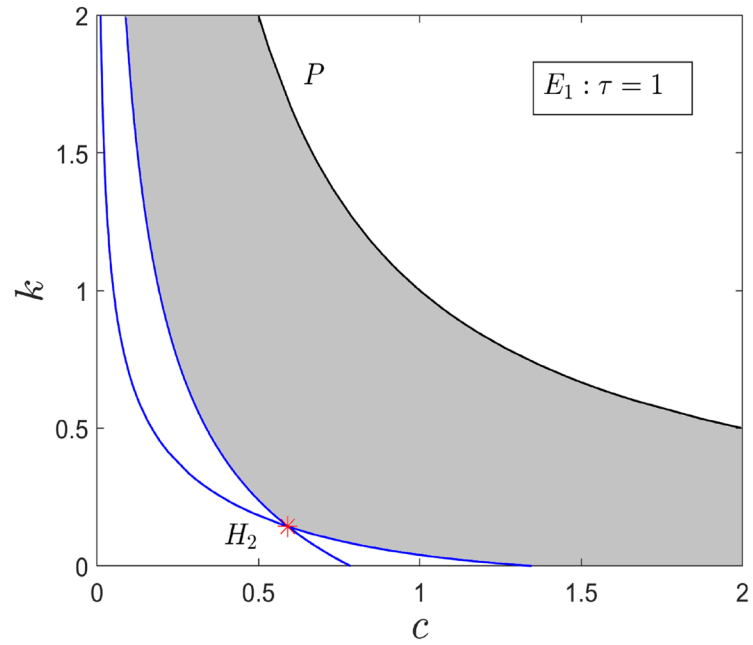

Fig. 4(c)

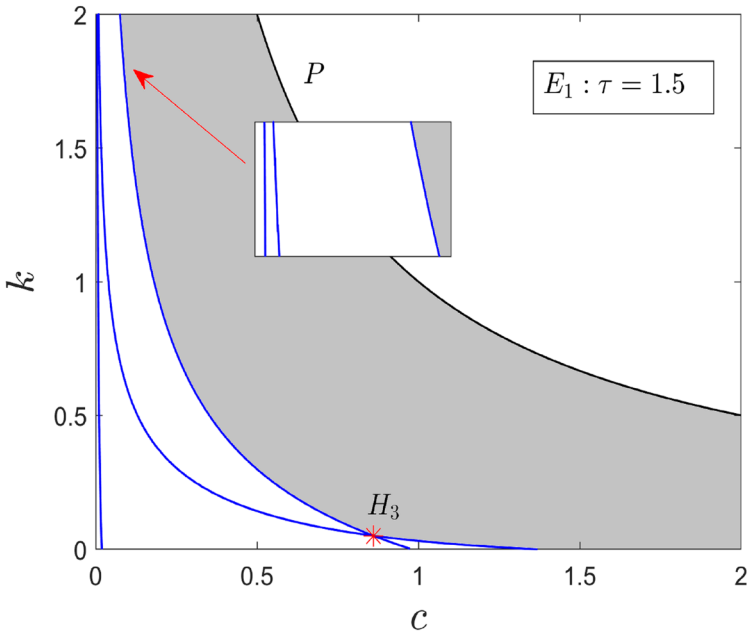

Fig. 4(d)

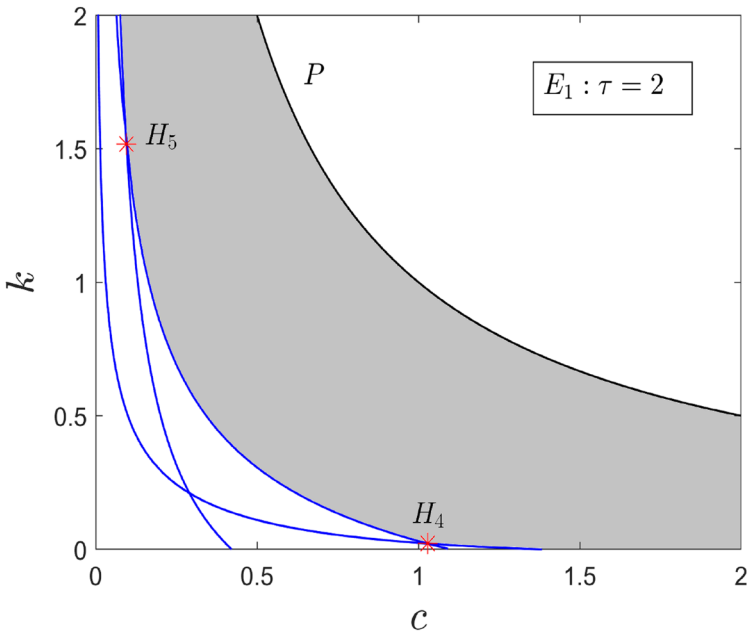

Fig. 4(e)

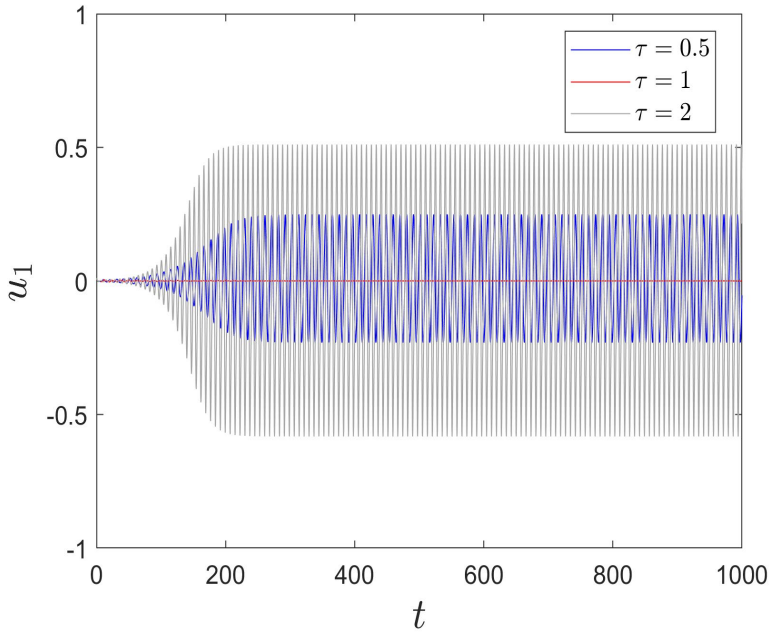
$\tau = 0.5$
$\tau = 1$
$\tau = 2$
u_1
t
1
0.5
0
-0.5
-1
0
200
400
600
800
1000

Fig. 5

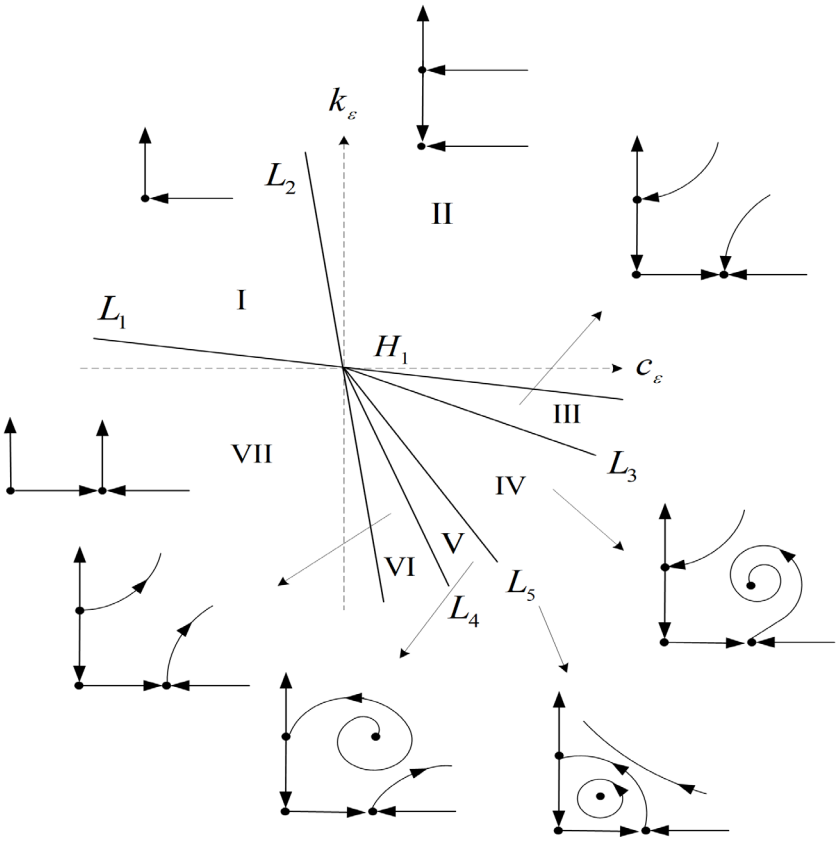
k_ε
L_2
II
I
L_1
H_1
c_ε
III
VII
L_3
IV
V
VI
L_4
L_5

Fig. 6

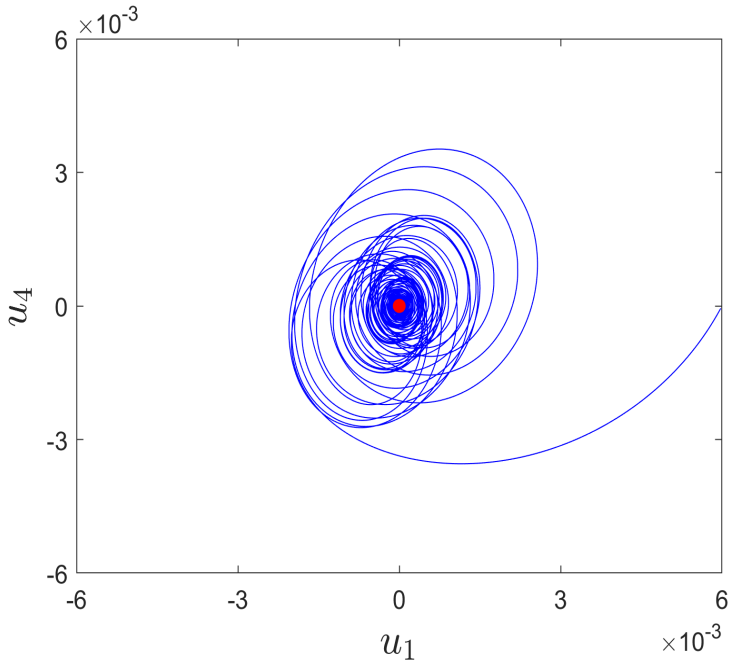

Fig. 7(a)

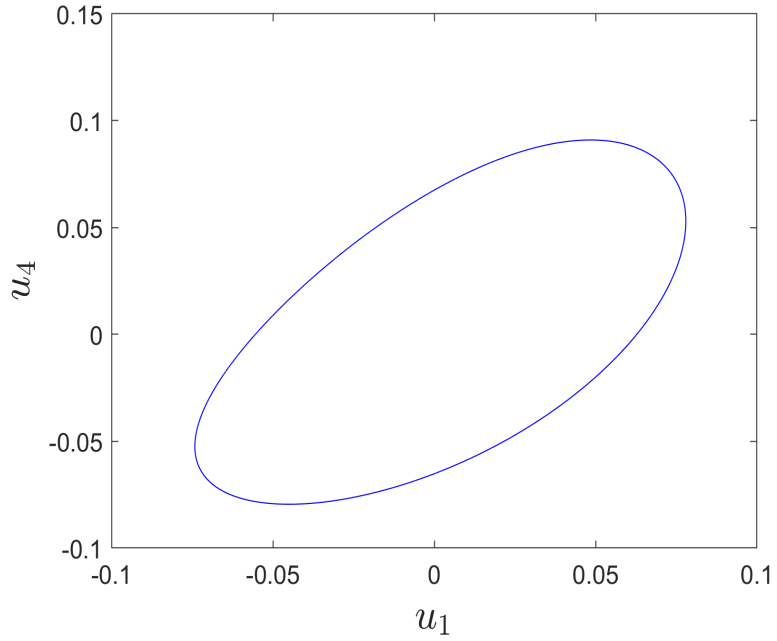

Fig. 7(b)

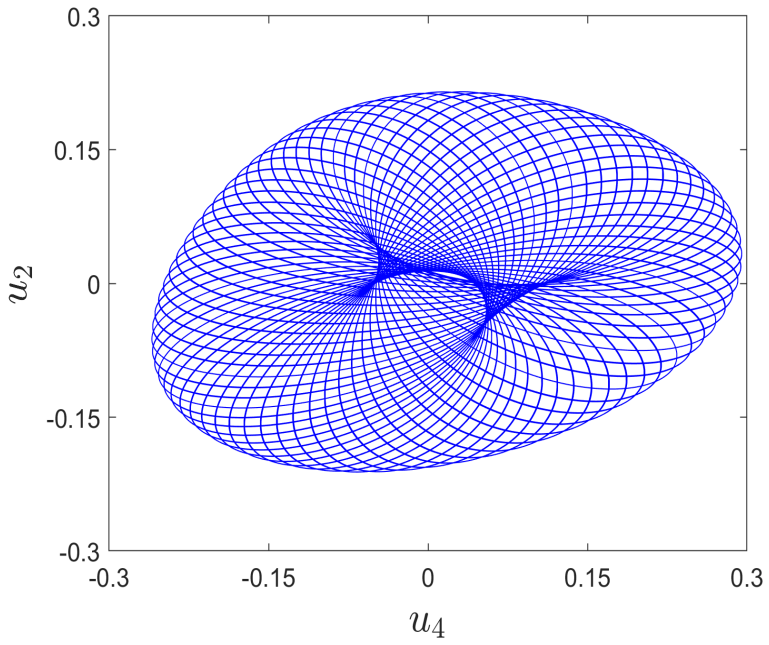
0.3
0.15
0
-0.15
-0.3
u_2
-0.3
-0.15
0
0.15
0.3
u_4

Fig. 7(c)

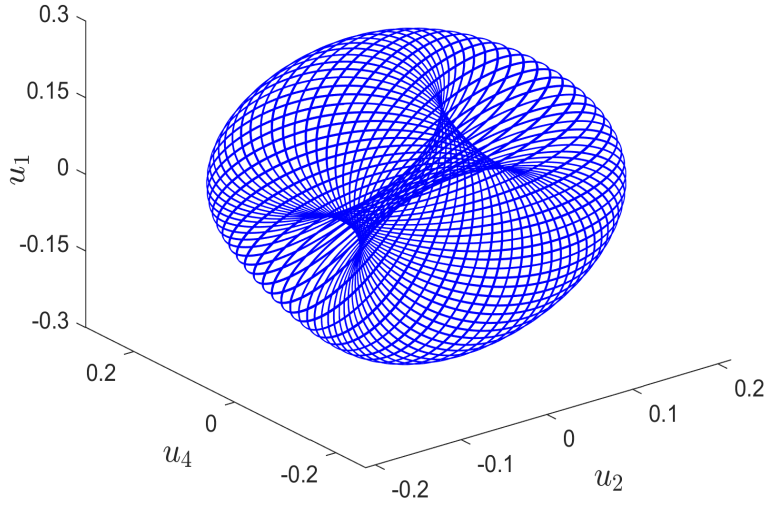
0.3
0.15
0
-0.15
-0.3
u_1
0.2
0
-0.2
u_4
-0.2
-0.1
0
0.1
0.2
u_2

Fig. 7(d)

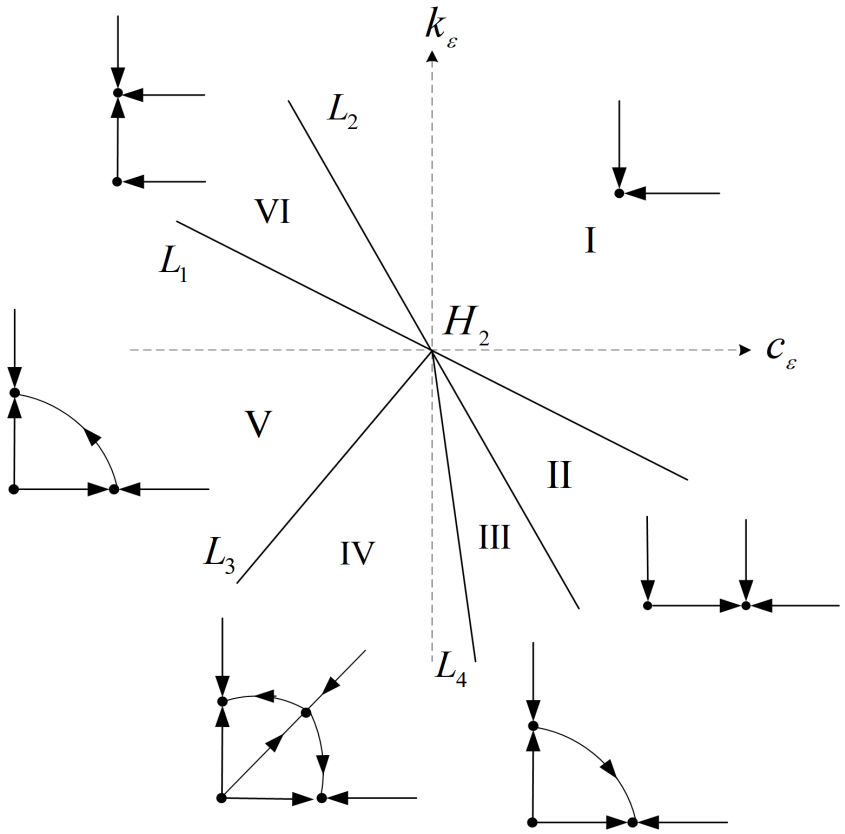
k_ε
L_2
VI
I
L_1
H_2
c_ε
V
II
L_3
IV
III
L_4

Fig. 8

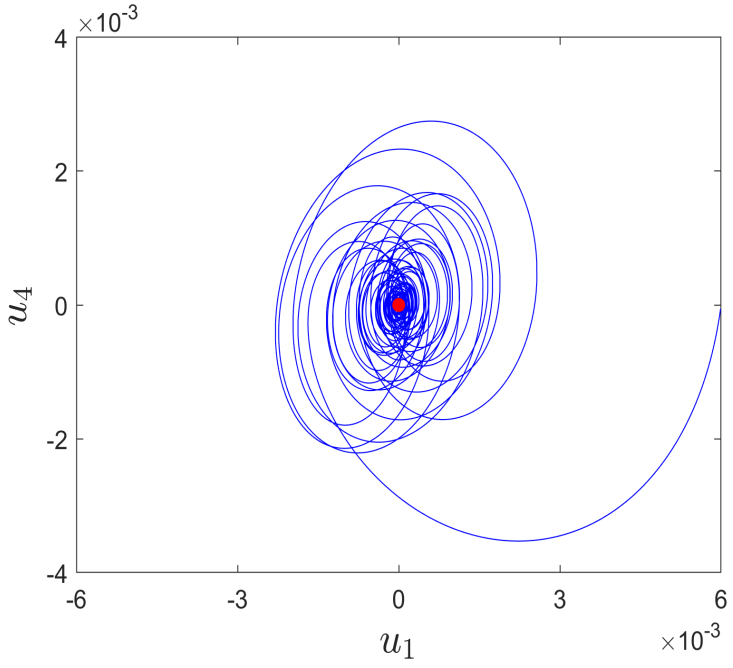
×10-3
4
2
0
-2
-4
u_4
-6
-3
0
3
6
u_1
×10-3

Fig. 9(a)

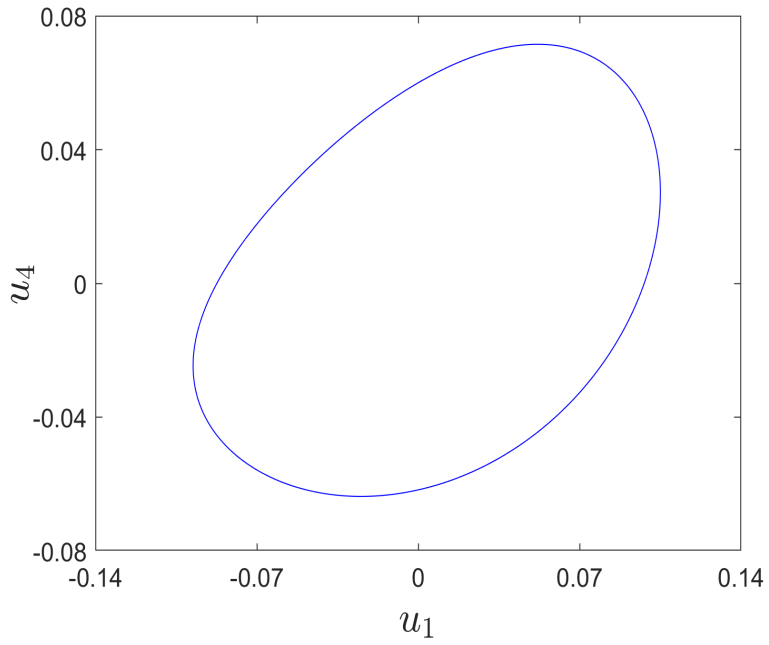
0.08
0.04
0
-0.04
-0.08
u_4
-0.14
-0.07
0
0.07
0.14
u_1

Fig. 9(b)

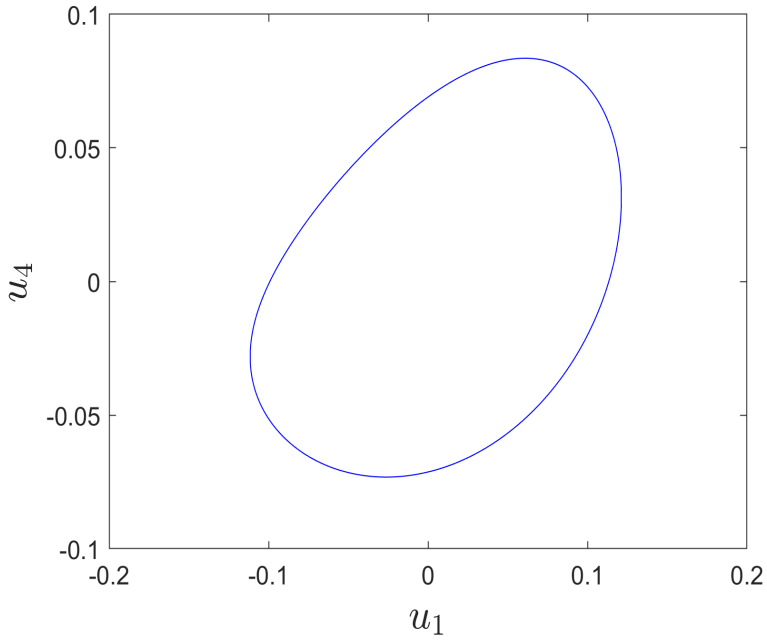
0.1
0.05
0
-0.05
-0.1
u_4
-0.2
-0.1
0
0.1
0.2
u_1

Fig. 9(c)

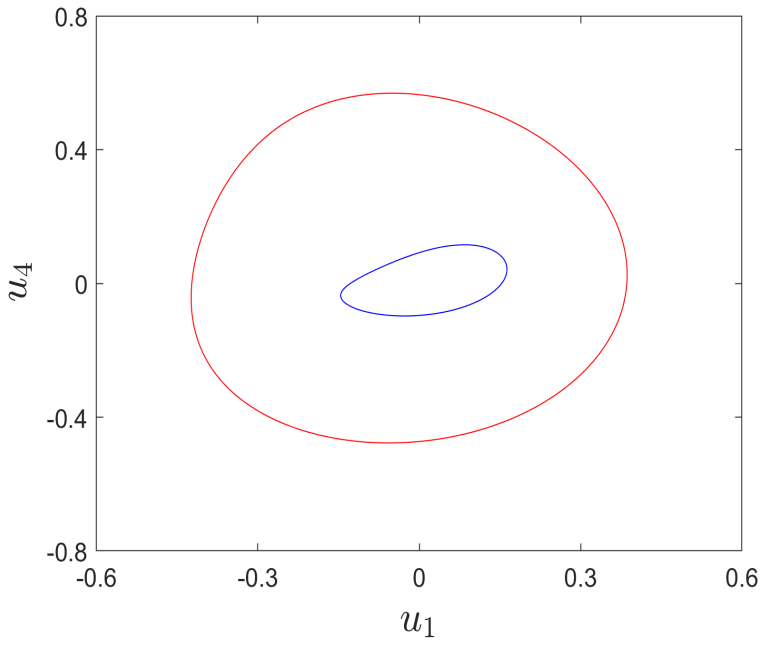

Fig. 9(d)

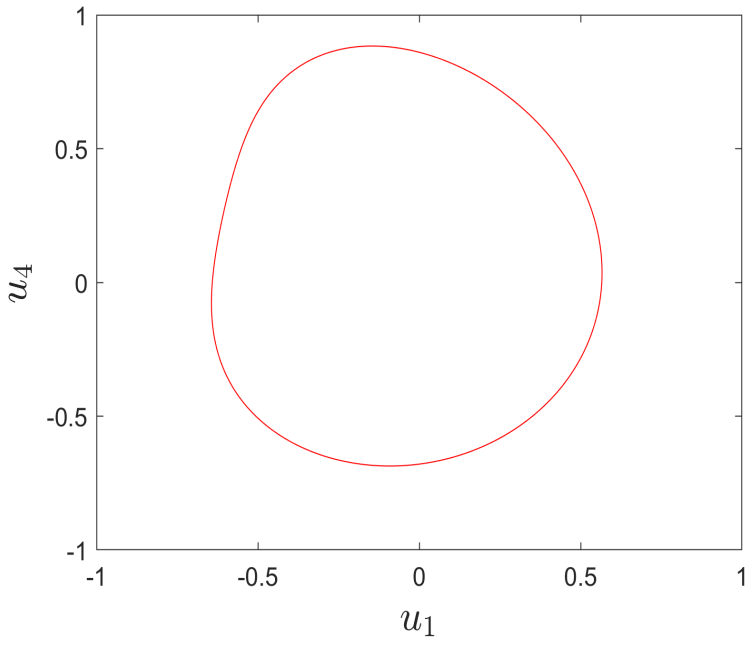

Fig. 9(e)

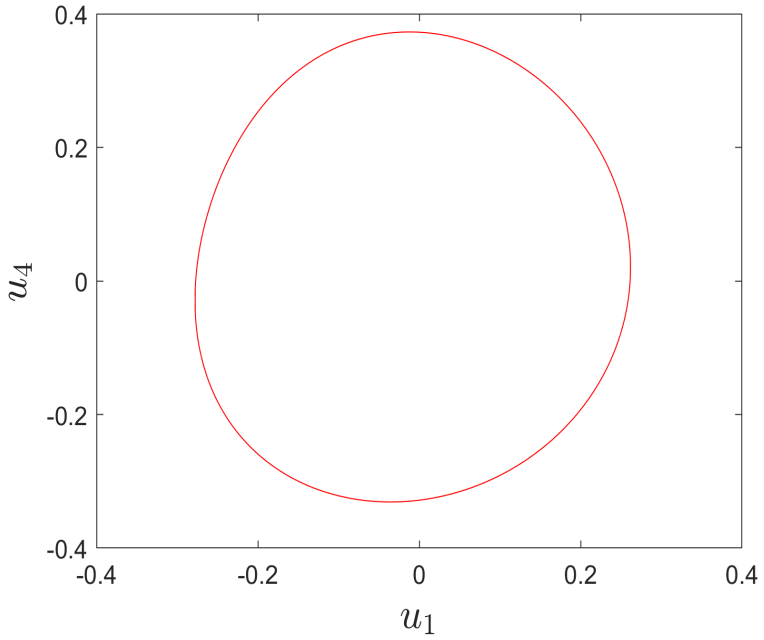
0.4
0.2
0
-0.2
-0.4
-0.4
-0.2
0
0.2
0.4
u_4
u_1

Fig. 9(f)

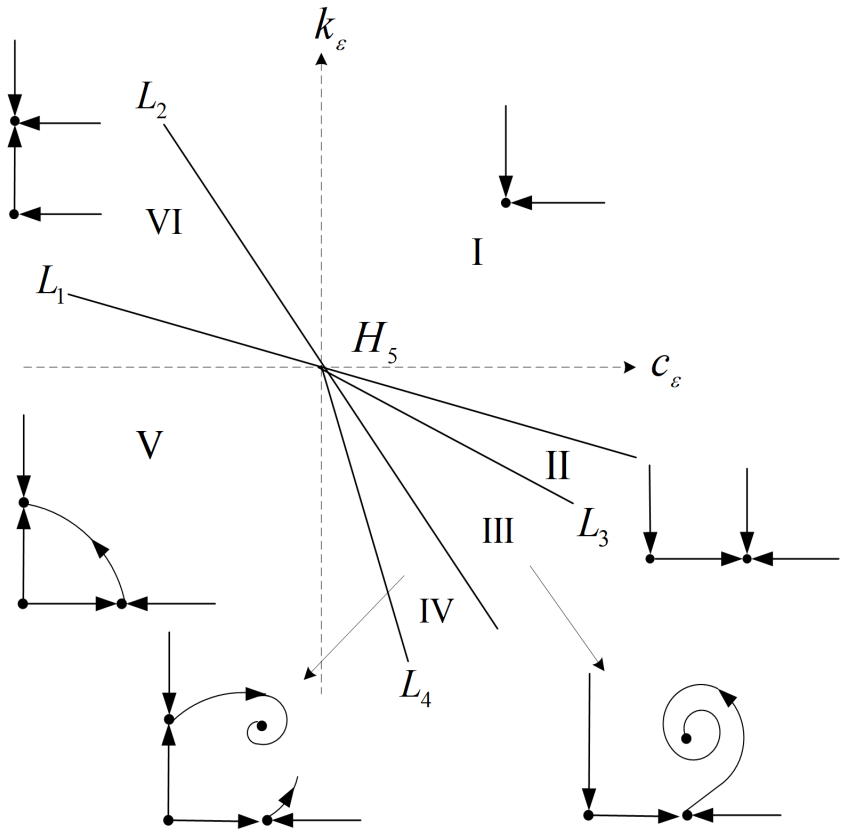
k_ε
L_2
VI
I
L_1
H_5
c_ε
V
II
L_3
III
IV
L_4

Fig. 10

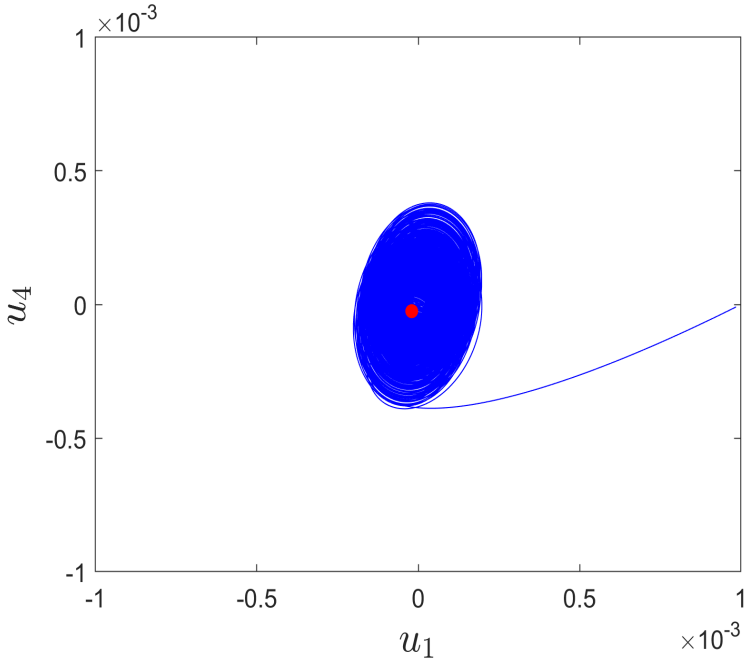

Fig. 11(a)

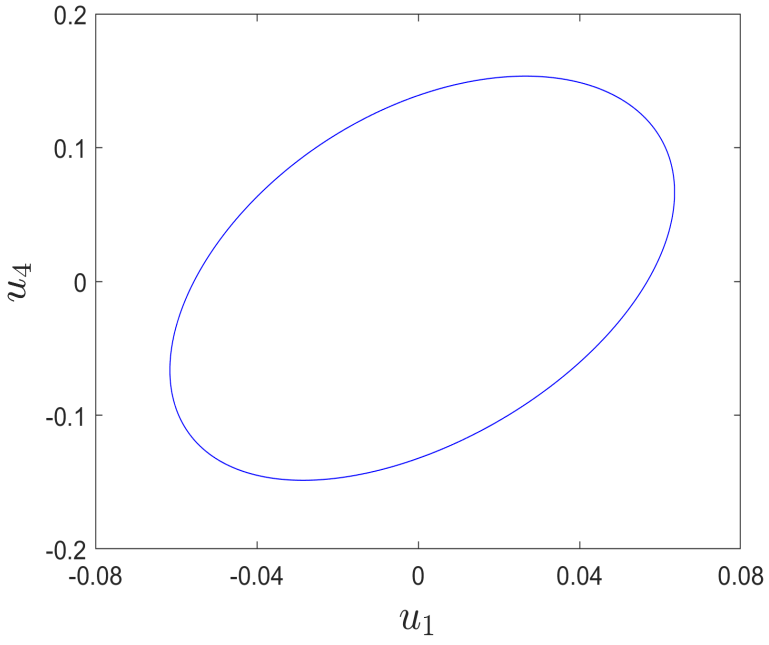

Fig. 11(b)

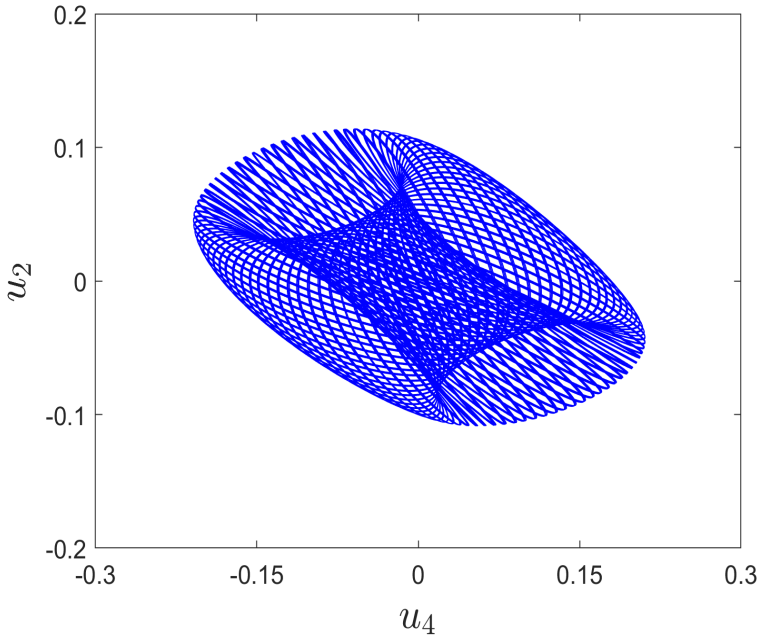

Fig. 11(c)

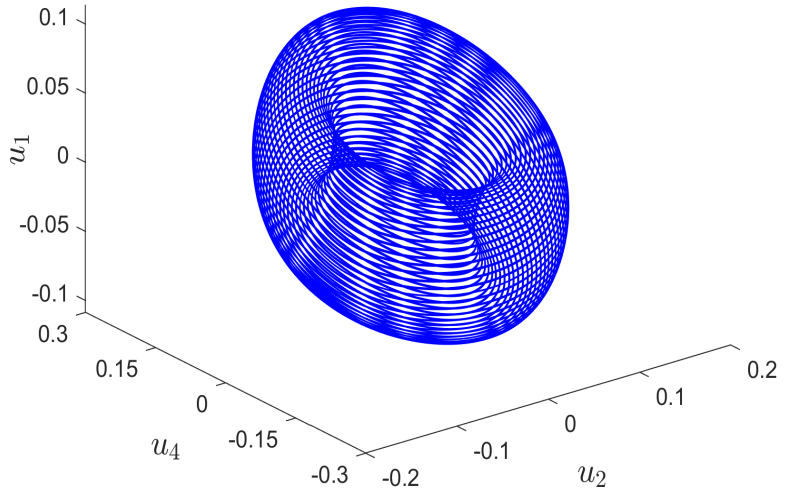

Fig. 11(d)

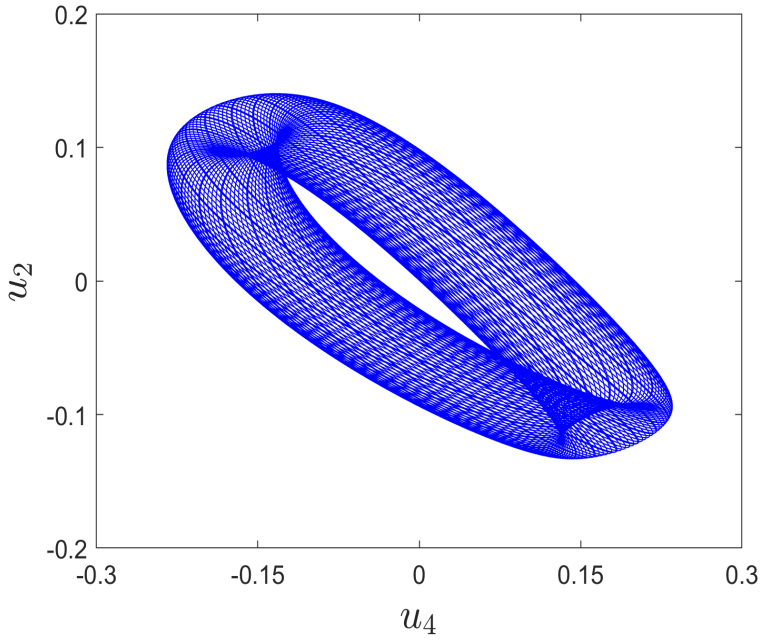

Fig. 11(e)

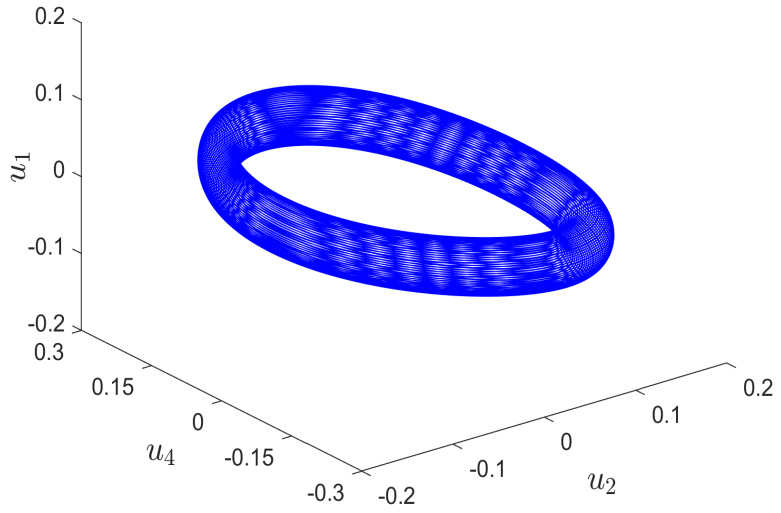

Fig. 11(f)

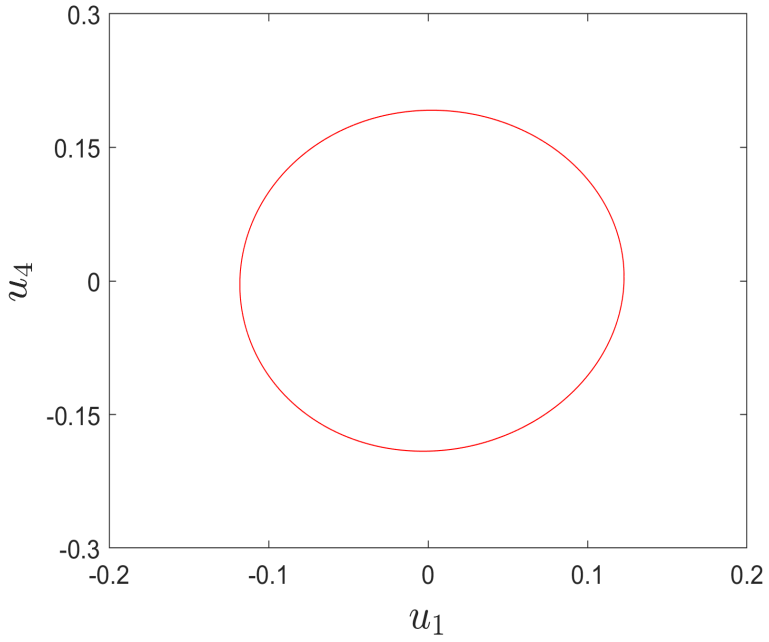

Fig. 11(g)

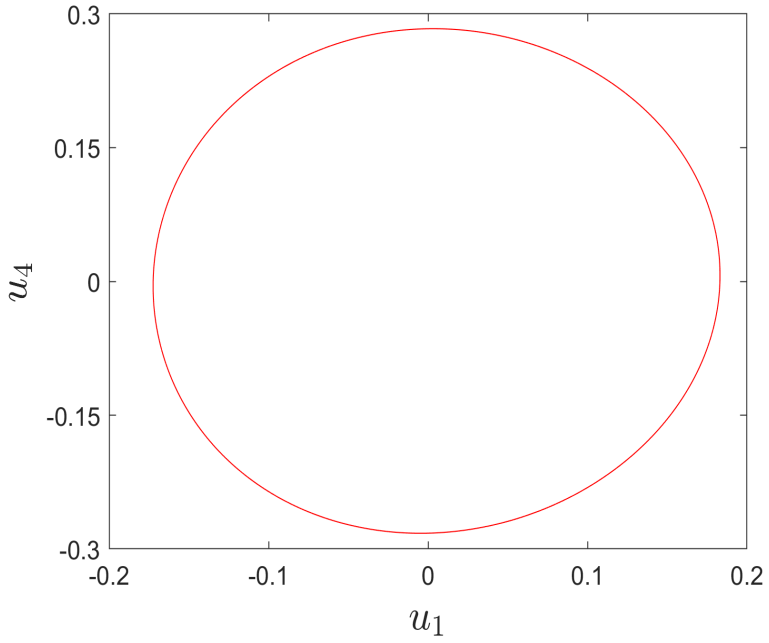

Fig. 11(h)

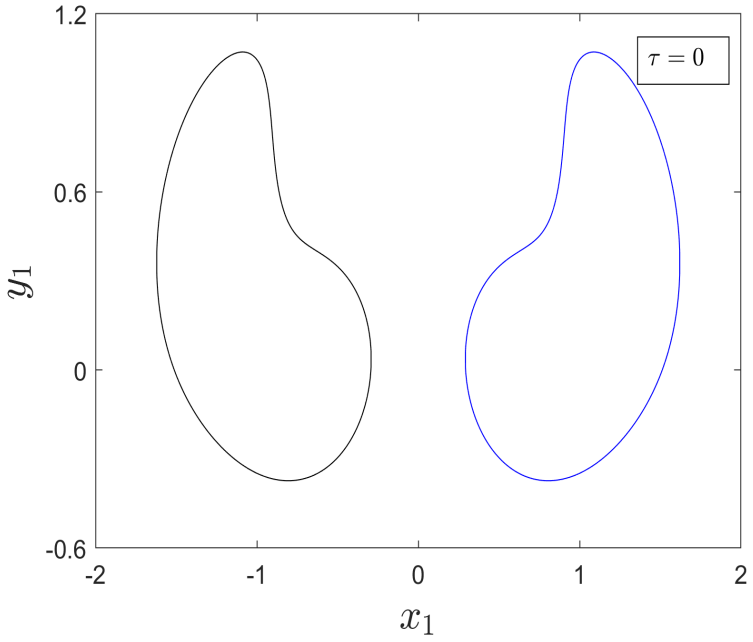

Fig. 12

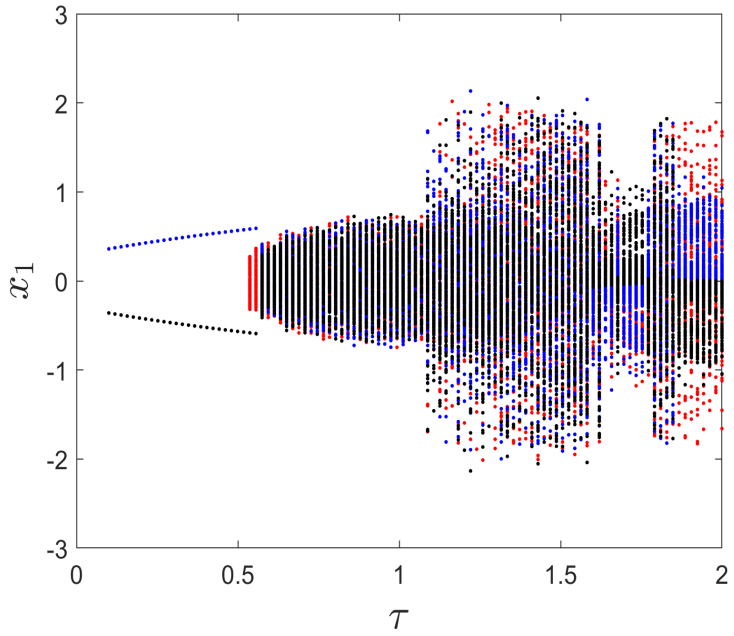

Fig. 13(a)

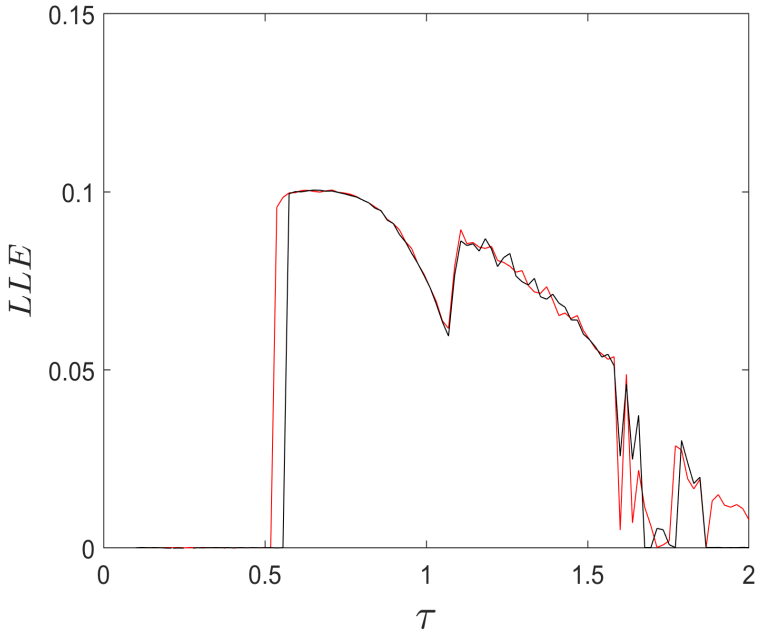

Fig. 13(b)

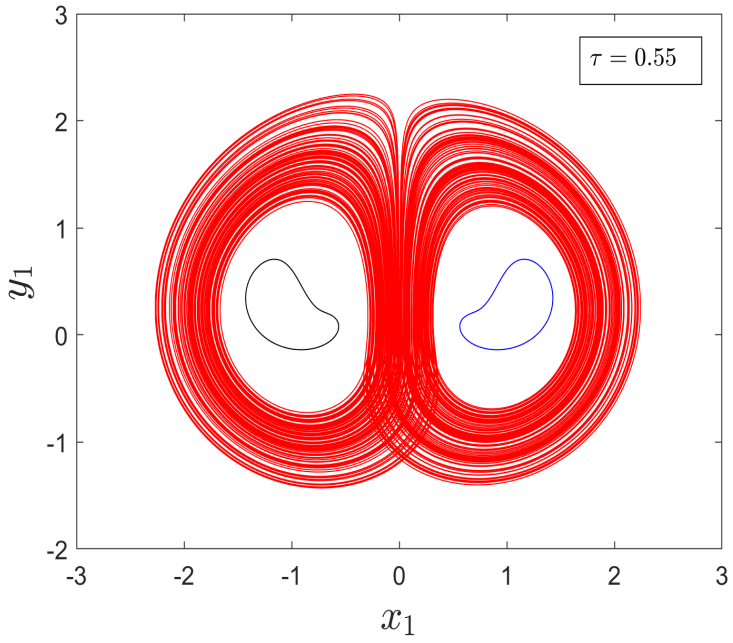

Fig. 14(a)

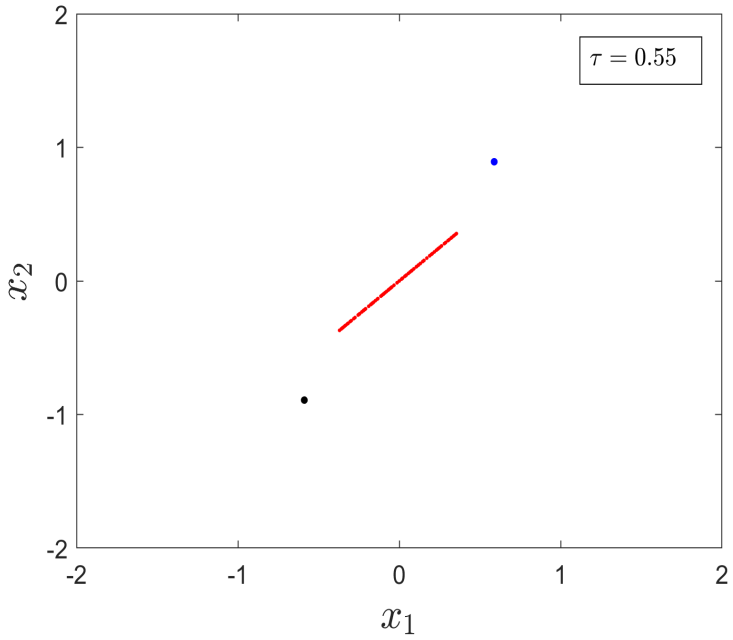

Fig. 14(b)

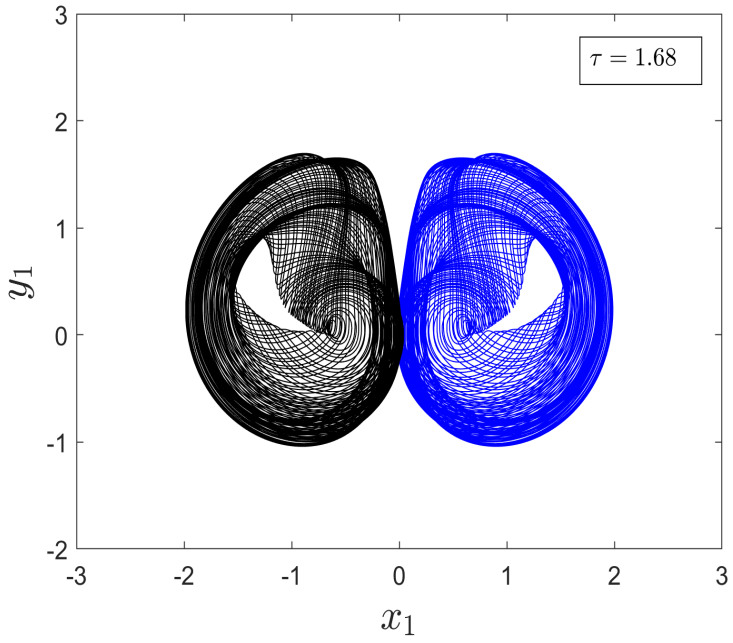

Fig. 14(c)

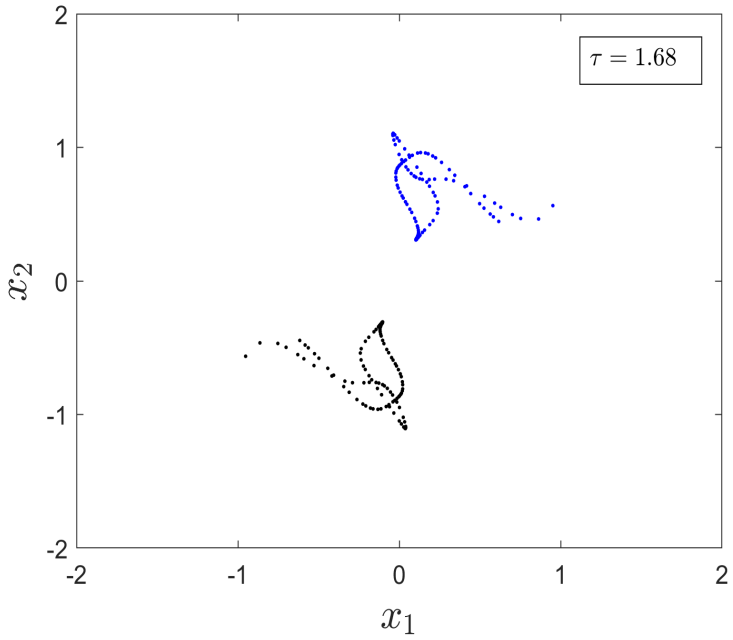

Fig. 14(d)

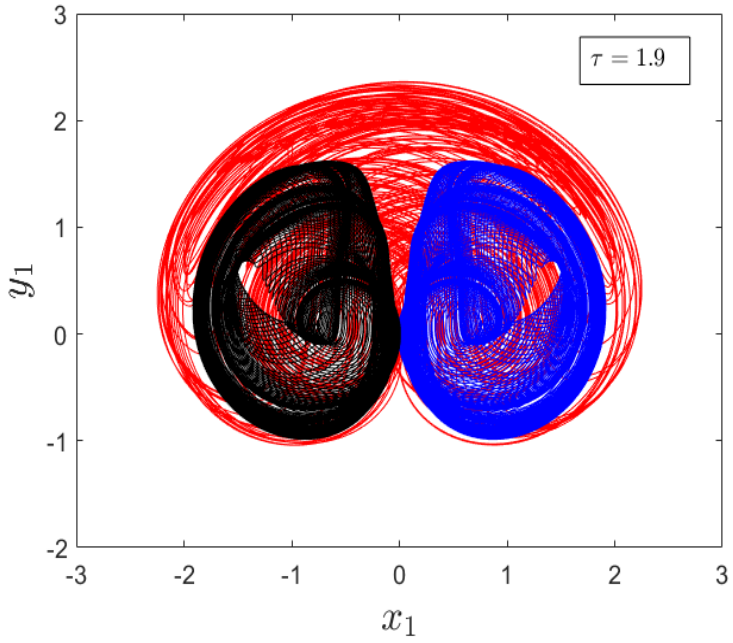

Fig. 14(e)

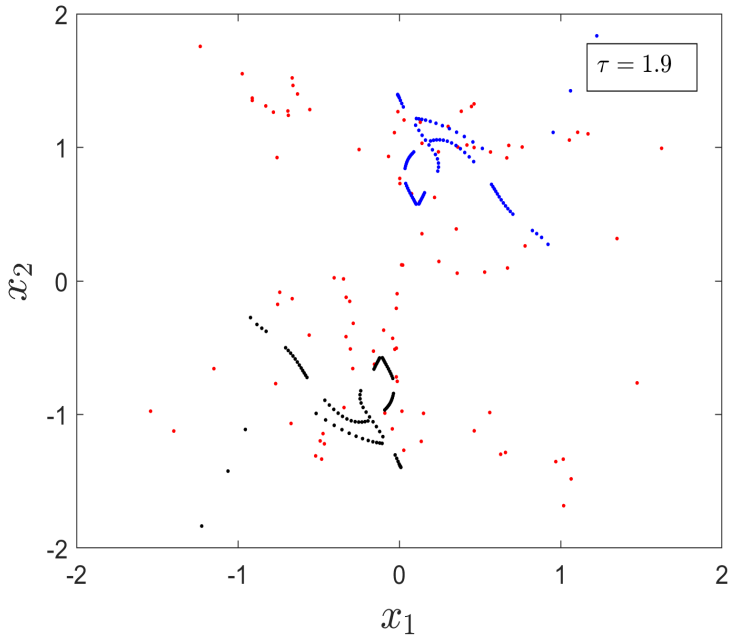

Fig. 14(f)